Dihydropyrene/Cyclophanediene Photoswitching Mechanism Revisited with Spin-Flip Time-Dependent Density Functional Theory: Nature of the Photoisomerization Funnel at Stake!

Elise Lognon, Rudraditya Sarkar, Marie-Catherine Heitz, Martial Boggio-Pasqua

Dihydropyrene / Cyclophanediene Photoswitching Mechanism Revisited with Spin-Flip Time-Dependent Density Functional Theory: Nature of the Photoisomerization Funnel at Stake!

Elise Lognon,[a] *Rudraditya Sarkar,*[a,b] *Marie-Catherine Heitz,*[a] *Martial Boggio-Pasqua*[a]*

[a] Laboratoire de Chimie et Physique Quantiques, FeRMI, Université Paul Sabatier, CNRS, Université de Toulouse, 31062 Toulouse, France

[b] Institut de Química Computacional I Catàlisi, Facultat de Ciències, University of Girona, C/ M. Aurèlia Campmany, 69, 17003 Girona, Spain

KEYWORDS. Photoisomerization, Photochromism, Conical Intersections, spin-flip DFT

ABSTRACT. The complex photoisomerization mechanism of the dihydropyrene (DHP) photochromic system is revisited using spin-flip time-dependent density functional theory (SF-TD-DFT). The photoinduced ring-opening reaction of DHP into its cyclophanediene (CPD) isomer involves multiple coupled electronic states of different character. A balanced treatment of both static and dynamic electron correlation is required to determine both the photophysical and

photochemical paths in this system. The present results provide a refinement of the mechanistic picture provided in a previous complete active space self-consistent field plus second-order perturbation theory (CASPT2//CASSCF) study based on geometry optimizations at the CASSCF level. In particular, the nature of the conical intersection playing the central role of the photochemical funnel is different. While at the CASSCF level, the crossing with the ground state involves a covalent doubly excited-state leading to a three-electron/three-center bond conical intersection, SF-TD-DFT predicts a crossing between the ground state and a zwitterionic state. These results are supported by multi-state CASPT2 calculations. This study illustrates the importance of optimizing conical intersections at a sufficiently correlated level of theory to describe photochemical path involving crossings between covalent and ionic states.

1. INTRODUCTION

Molecular photoswitches have emerged as fascinating chemical species that can be converted between at least two different isomeric forms in a controlled manner under external optical stimuli. These systems have been intensively developed over the past few decades because of their use in numerous important applications in the field of biology, nano and material sciences.[1,2,3,4,5,6,7,8,9,10,11,12,13] In order to control and optimize the properties and functions of these photoresponsive materials upon light irradiation, it is necessary to understand the underlying photoswitching mechanism of the molecular building blocks incorporated in these materials. Among them, organic photochromic systems have been largely used and investigated both from experimental and theoretical perspectives. They most often undergo either electrocyclization

reactions, cis/trans isomerizations, cycloadditions, proton transfer (i.e., tautomerism) or dissociation processes.[14]

Among the many photochromic molecules known to date,[14,15,16] derivatives of the dihydropyrene (DHP) family[17] deserve a special attention for multiple reasons. Under visible light irradiation, the π-conjugation of the quasi-planar DHP annulene core is lost during the formation of the cyclophanediene (CPD) open-ring isomer, which is characterized by a step-like structure with two benzene rings connected by two ethylene bridges (Scheme 1). The metastable CPD isomer can then be converted back to the stable DHP photochemically with UV light or thermally. The associated loss of π-conjugation upon DHP to CPD photoswitching has been exploited to controllably regulate the conductance in electronic devices and materials.[18,19,20,21,22,23,24] In addition, the aromatic DHP absorbs in the visible region, whereas the less aromatic CPD absorbs in the UV region, meaning that this system belongs to the less common class of negative photochromic systems. Because the stable DHP form absorbs at a longer wavelength than the metastable CPD isomer, it guarantees that continuous irradiation of DHP with visible light will not trigger the photochemical backward reaction. Moreover, it leaves open the possibility to excite the system with a low-energy irradiation, a feature of interest for biological applications. While the first synthesized DHPs suffered from poor thermal stability and photoswitching efficiency,[25,26,27] their chemical functionalizations using a variety of different strategies have led to improved systems.[28,29,30,31,32,33,34,35,36] DHPs have thus been exploited in the design of multistate switches,[37,38] mixed valence-state compounds,[39,40] hybrid systems for multifunctional materials[41,42,43,44,45,46] and devices for logic gates.[47] More recently, DHPs have also been considered for biological applications with systems operating in the biological window[48,49,50] and capable of producing singlet oxygen.[51,52,53]

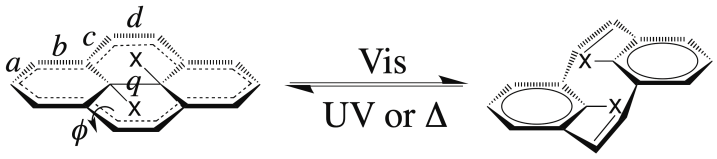

DHP **CPD**

1c X = H **1o** X = H
2c X = Me **2o** X = Me

Scheme 1. The dihydropyrene (DHP) / cyclophanediene (CPD) photochromic couple and labels used for geometrical parameters.

Besides the wide range of potential applications offered by the exploitation of DHPs photoswitching properties, these systems also represent a formidable challenge from the theoretical point of view. One of the major difficulties comes from the fact that the photoisomerization mechanism involves several coupled electronic excited states of various character (covalent and ionic, singly- and doubly-excited).[54,55] This type of complexity in the electronic wavefunctions usually requires using accurate multiconfigurational wavefunction-based quantum chemistry methods to account for both the static and dynamic electron correlation necessary to describe all these electronic states simultaneously in a balanced way. The most efficient and widely used method to deal with this type of study is the complete active space second-order perturbation theory (CASPT2)[56,57] and its multistate variant (MS-CASPT2).[58] Although being more than thirty years old, CASPT2 still stands as the gold standard in computational photochemistry because it appears as the most cost-effective ab initio method that can treat strong correlation.[59] Moreover, it has benefited over the years of various improvements for better reliability[60,61,62] and speed-up.[63,64,65,66] More recently, developments and implementation of analytic energy gradients[67,68,69,70,71,72] including derivative couplings[73] offer the thrilling opportunity to compute excited-state relaxation pathways travelling across conical intersections

(CIs)[74,75,76] and perform on-the-fly photodynamics simulations[77,78] at the MS-CASPT2 level.[79] However, one of the main limitations of this approach is tied up with the size of the reference active space and the number of correlated electrons in the perturbative treatment. The number of terms in the full configuration interaction expansion resulting from the distribution of the active electrons among the active orbitals in the complete active space self-consistent field (CASSCF) reference calculation grows exponentially with the size of the active space. The photoisomerization of DHP into CPD involves distributing 16 active electrons in 16 active orbitals, which can be handled at the MS-CASPT2 level for singlet-point energy calculations but is too demanding for the computation of energy gradients. Thus, the determination of the complex photoisomerization pathway for this system requires using a computationally more efficient strategy. In this context the spin-flip time-dependent density functional theory[80] (SF-TD-DFT) provides a powerful alternative to compute photochemical pathways involving CIs. In particular, this method can describe low-lying coupled singlet states including the closed-shell singlet ground-state, the open-shell singlet excited state and the doubly-excited closed-shell singlet state all important in the DHP/CPD photoisomerization (vide infra). The implementation of analytic energy gradients[80] and derivative couplings[81] has put this method at the center of the stage in the field of computational photochemistry, as non-adiabatic photochemical processes can be investigated both from static[82,83,84,85,86,87,88] and dynamic[89,90,91,92,93] perspectives, even for large molecular systems[94] or systems in condensed phase[93,95] when combined with a tight-binding formalism and/or a quantum mechanical/molecular mechanics scheme.

In this work, we have used SF-TD-DFT, supported by MS-CASPT2 calculations, to study the photoisomerization pathway of the DHP photochromic system based on static information provided by the exploration of the relevant potential energy surfaces and the analysis of the

associated electronic structures. Our results confirm the overall mechanism previously proposed[54] on the basis of CASPT2 calculations performed at CASSCF optimized geometries (denoted CASPT2//CASSCF), but also show some significant differences, most notably in the nature of the main photochemical funnel (i.e., CI) responsible for the DHP to CPD photoisomerization. This is a direct result of including the dynamic electron correlation in the optimization of the various critical structures, which was not assessed before for such a complex system, yet being a requirement to describe all the relevant electronic states of DHP/CPD. The article is organized as follows. In the next section, we present orbital and state correlation diagrams and recall the main mechanistic results from the previous CASPT2//CASSCF study.[54] A section reporting our computational strategy and details is then presented. We describe next the results of our SF-TD-DFT study, which are compared with accurate new MS-CASPT2 data and with the previous CASPT2//CASSCF results. The subtle change in the photoisomerization mechanism obtained upon including dynamic electron correlation is discussed, in particular regarding the nature of the photochemical funnel. A summary of the main results and some perspectives are given in conclusion.

2. MECHANISTIC PICTURE: FROM CORRELATION DIAGRAMS TO CONICAL INTERSECTIONS

Orbital and state correlation diagrams have long been used to provide an intuitive and qualitative picture of the isomerization mechanism in the ground and excited states of pericyclic reactions.[96] Based on simple correlations between the molecular orbitals of the reactant and product along a symmetry-preserving reaction coordinate, valuable information on the topology of the ground- and excited-state potential energy surfaces can be obtained, in particular regarding the presence or not

of potential energy barriers along the considered reaction coordinate in the respective electronic states.[97,98] The orbital and state correlation diagrams along the C_{2h} symmetry-preserving cycloreversion coordinate of DHP into CPD is shown in Figure 1. The frontier orbitals of the DHP reactant (HOMO–1: b_g; HOMO: a_g; LUMO: b_u and LUMO+1: a_u) are correlated with those of the CPD product (HOMO–1: b_g; HOMO: b_u; LUMO: a_g and LUMO+1: a_u), showing a crossing of the HOMO and LUMO energy levels (Fig. 1a). As a consequence, the ground electronic state $|\text{HOMO}\rangle^2$ of DHP correlates with the doubly excited state $|\text{LUMO}\rangle^2$ of CPD, and vice versa (Fig. 1b). Because these two electronic states are totally symmetric and belong to the same irreducible representation (A_g) of the C_{2h} symmetry point group, an avoided crossing between the 1^1A_g and 2^1A_g states is expected along the DHP→CPD isomerization coordinate. It thus appears that the thermal cyclization is a symmetry-forbidden process[31,99,100] but that the photocyclization in the $|\text{HOMO, LUMO}\rangle$ state is symmetry-allowed.

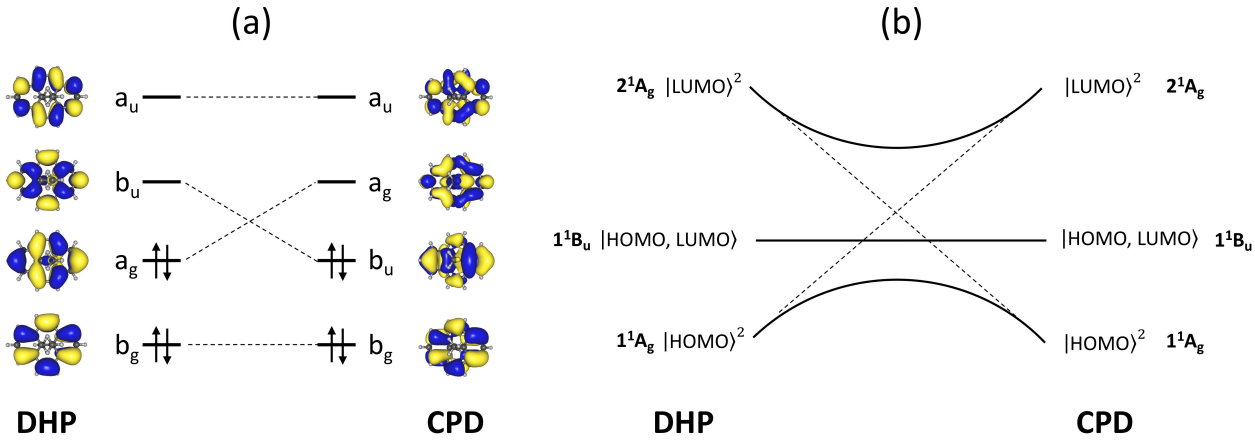

Figure 1. Orbital (a) and state (b) correlation diagrams for the DHP→CPD photoisomerization.

Because of their shortcomings, these correlation diagrams only provide an oversimplified mechanistic picture of the photoisomerization mechanism. They rely on the assumption that the reaction coordinate preserves the C_{2h} symmetry of the reactant (DHP) and product (CPD) in the

course of the photoisomerization. However, they give some important insight into the location of barriers and funnels (i.e., CIs) between electronic states. Fig. 1b shows that a barrier is present in the ground state due to the presence of a locally avoided crossing in C_{2h} symmetry. This avoided crossing also implies that a CI between the $|\mathrm{HOMO}\rangle^2$ and $|\mathrm{LUMO}\rangle^2$ electronic states is expected upon breaking the C_{2h} symmetry of the system. In addition, the $|\mathrm{HOMO, LUMO}\rangle$ state, which is predicted as a state predisposed for a barrierless photoisomerization, could also potentially cross the ground state. Thus, the pathway to the CI responsible for the DHP→CPD photoisomerization (photochemical funnel) needs to be characterized in order to understand the photoswitching mechanism of this photochromic system.

In 2007, some of us investigated the DHP (**2c**)→CPD (**2o**) photoisomerization mechanism based on CASPT2 calculations along the photoisomerization pathway estimated using CASSCF optimized structures.[54] Because of the high computational demand required to perform these calculations – the DHP/CPD electrocyclic reaction involves the reorganization of 16 electrons (14 π + 2 σ electrons in DHP / 16 π electrons in CPD) in 16 orbitals – only the lowest excited state of each irreducible representation were computed in C_{2h} symmetry (i.e., 2^1A_g, 1^1A_u, 1^1B_u, 1^1B_g) with state-specific CASPT2 calculations performed using a reduced (12e, 12o) reference active space and a polarized double-ζ quality basis set. The S_0/S_1 minimum energy conical intersection (MECI) was optimized at CASSCF level also using a reduced (12e, 12o) active space.

The mechanistic picture resulting from this CASPT2//CASSCF study is summarized in Figure 2. Potential energy profiles corresponding to relevant electronic states are represented along the (**2c**)→(**2o**) (Scheme 1) reaction coordinate (Rx). The initially-excited state is the bright $S_2(1^1B_u)$ state. It is dominated by a HOMO→LUMO transition and possesses a strong zwitterionic character.[54,55] Upon vibrational relaxation in this excited state, the system evolves to a CPD

precursor (denoted CPD* in Figure 2) characterized by an elongated transannular C–C bond and a loss of planarity of the DHP core relative to the ground-state structure. An easily accessible S_1/S_2 CI lies in the vicinity of the CPD* excited-state minimum providing an efficient funnel for non-radiative decay to the lower $S_1(1^1A_u)$ excited state. This state is a covalent excited state described as a combination of the HOMO–1→LUMO and HOMO→LUMO+1 excitations.[54,55] Population of this state leads to an excited-state minimum (DHP* and yellow curved arrow in Figure 2) with a similar structure as ground-state DHP. From DHP*, the system can deactivate back to the initial ground-state DHP either radiatively (fluorescence) or non-radiatively (internal conversion and intersystem crossing). Thus, population of $S_1(1^1A_u)$ does not lead to photoisomerization and this state is responsible for the DHP photophysics. To undergo the DHP to CPD ring-opening reaction, the system needs to reach a crossing between the photoreactive zwitterionic 1^1B_u state and the biradicaloid 2^1A_g excited state (S_1/S_2 CI in the middle of Figure 2). Upon population of this biradicaloid excited state, the system can then decay to the ground state at a nearby symmetry-broken S_0/S_1 MECI (photochemical funnel) allowing for product formation (purple curved arrow in Figure 2). This MECI was thus assigned to the crossing between states correlating with the two ^1A_g electronic states that show an avoided crossing in C_{2h} symmetry, as predicted by the correlation diagram (Figure 1b). This type of crossing belongs to a well-known class of CI involving three weakly coupled π-electrons, largely documented in the literature and also known as a three-electron/three-center bond CI showing a local triangular structure.[101,102,103,104,105,106,107]

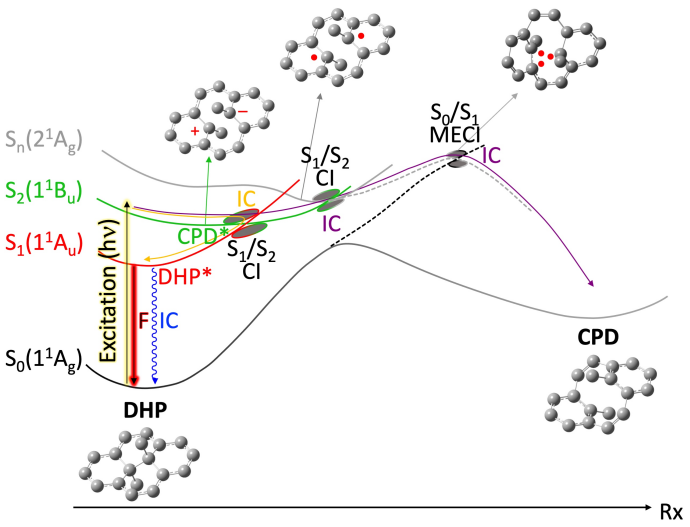

Figure 2. Schematic potential energy profiles of the relevant electronic states involved in the DHP/CPD photochromism based on CASPT2 energies along CASSCF adiabatic relaxation pathways. F: fluorescence, IC: internal conversion, (ME)CI: (minimum energy) conical intersection. Relevant structures for which hydrogen atoms have been omitted for clarity are shown. Yellow curved arrow: photophysical pathway; purple curved arrow: photoisomerization (photochemical) pathway. Color code of the potential energy curves based on the diabatic nature of the electronic states. Full lines correspond to potential energy curves along C_{2h} symmetry-preserving coordinates and dashed lines to a symmetry-breaking coordinate. Adapted from reference [108].

There is however one important limitation in this study due to the fact that it relied on CASPT2 energies computed along CASSCF relaxation pathways, a strategy which was considered state-of-the-art at that time. The effects of dynamic correlation on the DHP→CPD photochemical path was thus partly overlooked. These effects can prove to be crucial,[75,77,109,110] particularly when differential electron correlation is strongly dependent upon the inclusion of dynamic correlation. The location of conical intersections can then be highly sensitive to this correlation, as in the case of

ionic/covalent crossings.[111,112] This situation is indeed encountered in DHP/CPD for which several crossings involving the bright zwitterionic 1^1B_u state are travelled across along the photoisomerization pathway (see the two S_1/S_2 CIs shown in Figure 2). These crossings cannot be optimized using a CASPT2//CASSCF strategy and require using a quantum chemical method allowing the description of both the static and dynamic electron correlation and the computation of analytical energy gradients. In addition, the S_0/S_1 photochemical funnel optimized at the CASSCF level of theory is described as a covalent/covalent conical intersection. The two states that cross can be correlated to the two ^1A_g states in C_{2h} symmetry. However, the presence of the low-lying zwitterionic 1^1B_u state also raises the question of its possible implication in this photochemical funnel. We believe that the computational strategy that we describe next is well suited to overcome these difficult challenges.

3. COMPUTATIONAL STRATEGY AND DETAILS

3.1. Computational Strategy. Our strategy is based on the computation of the DHP (**1c**)→CPD (**1o**) photoisomerization path using SF-TD-DFT.[80] This approach relies on the use of a triplet reference state from which one-electron spin-flip excitations are generated. The main electronic configurations arising from such excitations in the four frontier orbitals are illustrated in Figure 3 for the **1c** DHP system. Excited states exhibiting double-excitation character are notoriously difficult to model using conventional single-reference methods.[113] One of the main advantages of SF-TD-DFT over TD-DFT is that the doubly-excited state 2^1A_g is physically well described, whereas it is completely missing from the one-electron excitation picture in TD-DFT. In addition, because the ground state 1^1A_g is determined from the same eigenvalue equation as the excited states, its mixing (and thus its multiconfigurational character) with the excited states, in particular

with the doubly-excited state 2^1A_g (as predicted by the correlation diagrams and the previous CASPT2//CASSCF study) and with the zwitterionic 1^1B_u state in case of symmetry breaking, will be naturally described. This feature is also lacking at the TD-DFT level. On the other hand, Figure 3 shows that the 1^1A_u state is spin-incomplete in SF-TD-DFT, meaning that this state will suffer from a strong spin-contamination. Thus, we expect SF-TD-DFT to be suitable to describe the photochemical (photoisomerization) path of DHP to CPD (purple curved arrow in Figure 2), which cannot be described at the TD-DFT level. However, the photophysical path (yellow curved arrow in Figure 2) may be less reliable due to the spin-contaminated 1^1A_u state. Note that the spin contamination issue of the 1^1A_u state can be cured using a mixed-reference (MR) spin-flip approach.[114] Although not required for the purpose of this study, which focuses mainly on the photochemical path (vide infra), we have used MR-SF-TD-DFT to assess the effect of spin-contamination on our SF-TD-DFT results. Note that TD-DFT is nicely suited to describe this photophysical path, as both the 1^1B_u and 1^1A_u states are physically well described in the one-electron excitation picture.[36]

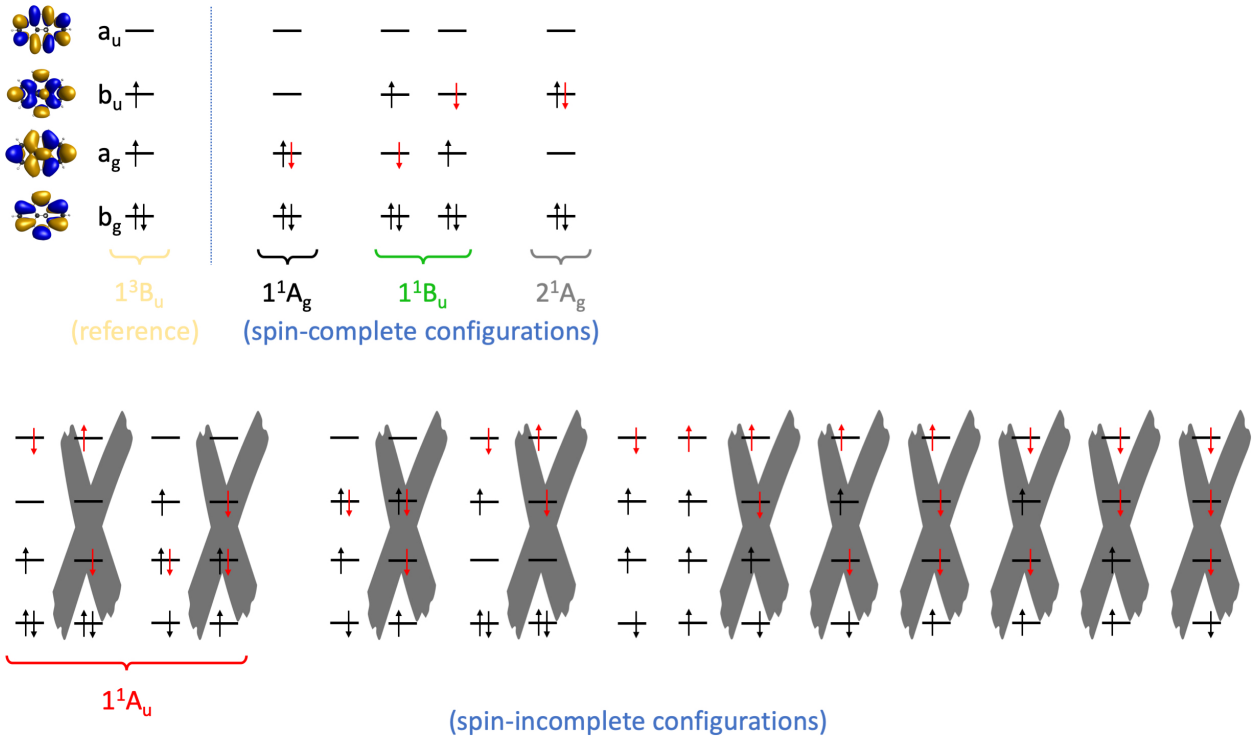

Figure 3. Representation of the electronic configurations (Slater determinants) obtained by one-electron spin-flip excitations from the reference triplet (shown without gray crosses) and the missing electronic configurations (shown with gray crosses) required to obtain configuration state functions. The labels of the main electronic states of DHP are represented.

We have thus computed the photochemical path at the SF-TD-DFT level considering relaxation in the two states involved in the DHP→CPD photoisomerization mechanism: the zwitterionic 1^1B_u and the doubly-excited 2^1A_g states. Minima and conical intersections were optimized and their structures were used to construct the photoisomerization path. A similar work was performed at the CASSCF level for the sake of comparison. MS-CASPT2 calculations were then performed along both the SF-TD-DFT and CASSCF relaxation pathways in order to assess the reliability of the proposed photoisomerization mechanism. In particular, these MS-CASPT2 results provide a

way to settle the different mechanistic pictures obtained at the SF-TD-DFT and CASPT2//CASSCF levels.

3.2. Computational Details. SF-TD-DFT calculations were performed within the Tamm-Dancoff approximation using both spin-restricted and spin-unrestricted triplet references. Because spin contamination of the reference triplet state propagates to the target singlet states, spin contamination of the spin-flip states will be more severe in the spin-unrestricted formalism. On the other hand, spin-restricted calculations are more prone to convergence difficulties. In the following, SF-TD-DFT results in the spin-restricted formalism are presented unless otherwise stated. All the results obtained in the spin-unrestricted formulation and with the MR-SF-TD-DFT are given in Supporting Information. All these calculations were performed with a half-and-half functional, BHHLYP,[115] with which best performances have been reported.[80,82,87,116] The chosen orbital basis is the 6-311G(d,p) basis set,[117] already used in previous DFT and TD-DFT studies of DHPs.[35,36,118,119] Frequency calculations were performed only in the spin-unrestricted formalism as available in Q-CHEM 5.2[120] in order to verify the nature of the stationary points (minimum and transition states). All the spin-restricted calculations were performed with GAMESS.[121] TD-DFT calculations were also performed with Q-CHEM 5.2 using the B3LYP functional[122] and the same basis set.

CASSCF calculations were performed including 16 active electrons in 16 active orbitals (14 π + 2 σ electrons in DHP / 16 π electrons in CPD), as required for the description of the electrocyclic DHP→CPD reaction. The various minima were optimized within the C_{2h} symmetry point group using state-specific CASSCF calculations with the MOLPRO 2019 package.[123] The S_0/S_1 MECI was optimized with state-averaged (SA-)CASSCF calculations without symmetry constraint.

Because the (16e, 16o) active space generates too many configurations in the C_1 point group, we had to use a reduced (12e, 12o) active space for the location of the MECI by removing the two orbitals with the highest average occupation numbers and the corresponding two orbitals with the lowest average occupation numbers from the (16e,16o) active space, as carried out in ref 54. MS-CASPT2 calculations were performed on top of SA-CASSCF(16,16) calculations using the MOLCAS package. SA-CASSCF calculations were performed by state-averaging over two ^1A_g, three ^1A_u, three ^1B_u and three ^1B_g states when C_{2h} symmetry was imposed. MS-CASPT2 calculations were then performed using the recommended standard IPEA shift[62,124,125] of 0.25 a.u. and an imaginary level shift[61] of 0.1 a.u. was chosen in order to minimize intruder state contributions. The Cholesky decomposition[64] of the two-electron integrals with a threshold of 10^{-6} a.u. was used to reduce the computational cost. For the path leading to the non-symmetrical S_0/S_1 MECI, a state-averaged procedure over five states was applied. A restricted-active space self-consistent field (RASSCF) reference was used to reduce the number of configurations generated by the (16e,16o) active space and MS-RASPT2 calculations were performed on top of this reference wavefunction.[126,127] The RAS2 (full configuration interaction) partition is made of the four frontier orbitals shown in Figure 3. The remaining six occupied and six virtual orbitals compose the RAS1 and RAS3 spaces, respectively, in combination with an excitation level including single and double excitations.

Minima on the respective potential energy surfaces and relevant conical intersections were fully optimized. Potential energy profiles were computed along linearly-interpolated in internal coordinates (LIIC) paths connecting the relevant critical structures. The LIIC paths were generated from both the CASSCF and SF-TD-DFT optimized structures, producing two distinct photochemical relaxation pathways. The MS-CASPT2 (and MS-RASPT2) calculations were then

performed along these LIIC paths, providing a way to assess the reliability of the SF-TD-DFT photochemical path. The cc-pVTZ basis set[128] was used throughout for all CASSCF, MS-CASPT2 and MS-RASPT2 calculations.

Third-order coupled cluster (CC3)[129] calculations with the cc-pVTZ basis set were performed at the ground-state CASSCF optimized geometry of the **1c** DHP system in order to provide reference vertical transition energies (VTEs). This level of theory provides highly accurate VTEs for excited states with a dominant single-excitation character.[113,130,131,132,133,134] These calculations were carried out using CFOUR.[135]

4. RESULTS AND DISCUSSION

4.1. Electronic structures and vertical transition energies. In this section, we describe in more details the electronic structures of the first six singlet excited states and compare the results provided by SF-TD-DFT against accurate reference methods such as MS-CASPT2 and CC3. The results of the VTEs and of the excitations involved are compiled in Table 1. As described earlier, the first two excited states are the $S_1(1^1A_u)$ and $S_2(1^1B_u)$ states. The first one is described as a nearly equal mixture of HOMO–1→LUMO and HOMO→LUMO+1 excitations, while the second one is dominated by a HOMO→LUMO excitation with some weaker contribution of the HOMO–1→LUMO+1 excitation. While SF-TD-DFT cannot rigorously describe the $S_1(1^1A_u)$ state because of spin-incompleteness (see Section 3.1) resulting in a high spin contamination ($\langle S^2 \rangle = 1.06$) due to a mixture of singlet and triplet A_u states, it yet describes correctly the mixture of HOMO–1→LUMO and HOMO→LUMO+1 excitations with respective configuration interaction coefficients of +0.64 and –0.72 in good agreement with CASSCF (see Table 1). In addition, the associated VTE is surprisingly in very good agreement with MS-CASPT2 and CC3. While this is

obviously fortuitous and due to error compensations, we will see in the following that SF-TD-DFT also provides a reasonable description of the photophysical pathway involving this state. With SF-TD-DFT, the $S_2(1^1B_u)$ state is located about 0.3 eV above the most accurate CC3 VTE of 3.02 eV, while MS-CASPT2 underestimates this reference value by 0.3 eV. This state is completely dominated (94% of the wavefunction) by the HOMO→LUMO excitation at the SF-TD-DFT level due to the fact that the HOMO–1→LUMO+1 excitation cannot be generated by a one-electron spin-flip excitation, accounting for both the low spin contamination of this state ($<S^2> = 0.07$) and the fact that it is too high in energy. The next two excited states are $S_3(2^1A_u)$ and $S_4(2^1B_u)$. $S_3(2^1A_u)$ is described as the in-phase combination of HOMO–1→LUMO and HOMO→LUMO+1 excitations with respective configuration interaction coefficients of +0.74 and +0.66 again in good agreement with CASSCF. For the same reason (spin-incompleteness) as for $S_1(1^1A_u)$, a high spin contamination ($<S^2> = 1.01$) is obtained, yet with a reasonable VTE close to the MS-CASPT2 value. The $S_4(2^1B_u)$ is dominated by the HOMO–1→LUMO+1 excitation and thus cannot be described with SF-TD-DFT. Finally, the next two states are the $S_5(1^1B_g)$ and $S_6(2^1A_g)$ dark (symmetry-forbidden) excited states. They both involve a mixture of one-electron and two-electron excitations. The main excitations that come out the SF-TD-DFT calculation for the $S_5(1^1B_g)$ state are HOMO→LUMO+2, HOMO–2→LUMO, $HOMO^2$→(LUMO)(LUMO+1) and (HOMO–1)(HOMO)→$LUMO^2$ with respective coefficients of +0.58, –0.49, +0.48 and –0.39. This is also consistent with the CASSCF result and the excitation energy is again surprisingly good considering the high spin contamination ($<S^2> = 1.03$) due to the spin incompleteness. The $S_6(2^1A_g)$, which is dominated by the $HOMO^2$→$LUMO^2$ excitation at the CASSCF level, is mainly described by the following excitations in SF-TD-DFT: (HOMO–1)(HOMO)→(LUMO)(LUMO+1), HOMO–3→LUMO, $HOMO^2$→$LUMO^2$ and

HOMO→LUMO+4 with respective coefficients of 0.57, 0.50, 0.42, 0.33. While the last three excitations are also found to substantially contribute to the CASSCF wavefunction, the first double excitation found in SF-TD-DFT has only a small contribution at the CASSCF level with a coefficient of –0.09. Although $S_6(2^1A_g)$ also suffers from spin-incompleteness and a strong spin contamination ($\langle S^2 \rangle = 1.18$), the VTE to this state is within 0.1 eV of the MS-CASPT2 and CC3 values. As a side note, one can remark that CASPT2 outperforms MS-CASPT2 for the VTEs using the CC3 values as reference. The CC3 VTE values are also probably not highly accurate for the $S_5(1^1B_g)$ and $S_6(2^1A_g)$ states, which share substantial double excitation character.

Table 1. Vertical transition energies (eV) and electronic configurations for DHP **1c**.

State	Excitation[a]	Config. coeff.[b]	CASSCF	CASPT2	MS-CASPT2	SF-TD-DFT	CC3
$S_0(1^1A_g)$	–	–	0	0	0	0	0
$S_1(1^1A_u)$	H–1→L	+0.56	1.842	2.075	2.067	2.187	2.057
	H→L+1	–0.54					
$S_2(1^1B_u)$	H→L	–0.76	4.633	2.802	2.712	3.300	3.022
	H–1→L+1	–0.44					
$S_3(2^1A_u)$	H→L+1	–0.59	5.446	3.310	3.221	3.157	3.562
	H–1→L	–0.56					
$S_4(2^1B_u)$	H–1→L+1	+0.64	6.012[c]	4.176	3.611	–	4.102
	H→L	–0.38					
$S_5(1^1B_g)$	H^2→(L)(L+1)	–0.37	3.994	4.084	4.075	4.150	4.233
	H–2→L	+0.37					
	(H–1)(H)→L^2	–0.34					
	H→L+2	+0.33					

$S_6(2^1A_g)$	$H^2 \rightarrow L^2$	+0.46	3.990	4.140	4.140	4.256	4.388
	H–3→L	+0.36					
	H→L+4	+0.31					
	$(HOMO–1)^2 \rightarrow (LUMO+1)^2$	–0.26					
	HOMO–2→LUMO+1	–0.21					

[a] Main electronic excitations based on CASSCF configurations. H = HOMO, L = LUMO. [b] CASSCF configuration interaction coefficients corresponding to the electronic excitations obtained from state-averaged canonical orbitals. [c] Corresponds to 3^1B_u at CASSCF level.

4.2. Relaxation pathway along the bright 1^1B_u excited state. Because the DHP→CPD photoisomerization is initiated by excitation to the $S_2(1^1B_u)$ state, we first explore the relaxation pathway on the corresponding potential energy surface. Figure 4 collects potential energy profiles of the different electronic states along the relaxation path of the 1^1B_u state. These profiles have been computed at the SF-TD-DFT level and at the MS-CASPT2 level using the LIIC path obtained from SF-TD-DFT optimized geometries (see Figure S1 in SI for SF-TD-DFT profiles computed in the spin-unrestricted formulation and Figure S2 for MR-SF-TD-DFT profiles). The MS-CASPT2 profiles have also been computed along the LIIC path obtained using CASSCF optimized geometries for the sake of comparison (Figure S3 in SI). The LIIC relaxation path is obtained by interpolating between the DHP ground-state minimum, the 1^1B_u excited-state minimum and the CPD ground-state minimum structures.

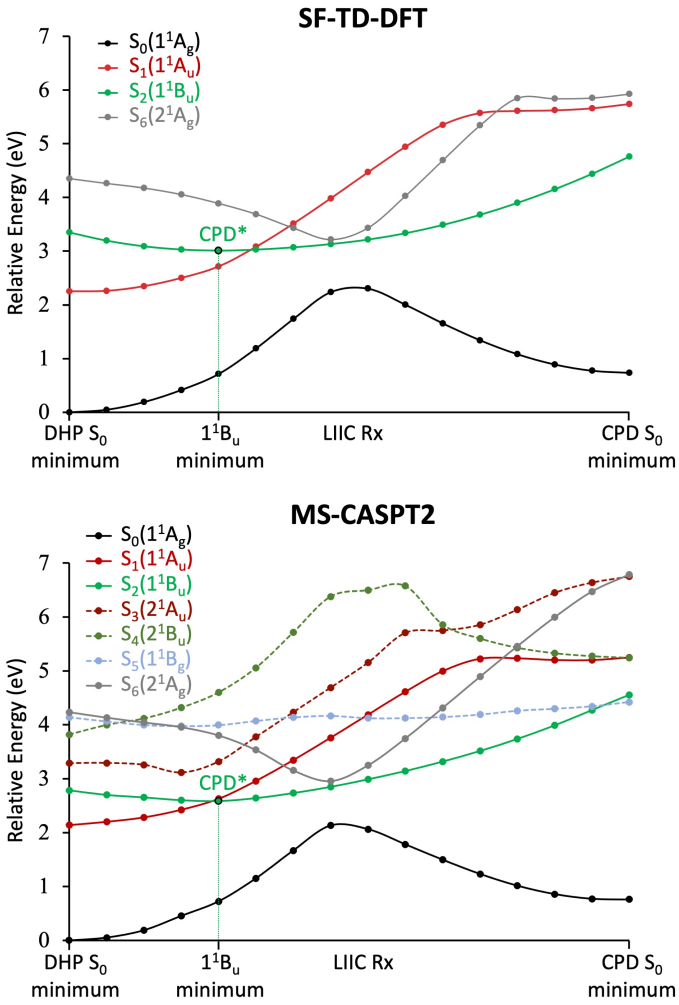

Figure 4. Potential energy profiles along the LIIC reaction path describing the approximate 1^1B_u relaxation pathway using SF-TD-DFT optimized structures. SF-TD-DFT results for the four relevant electronic states are shown (top) and MS-CASPT2 results for all states from S_0 to S_6 are shown (bottom). Dashed lines correspond to states not computed at SF-TD-DFT level. Color code based on symmetry labels.

As previously reported,[36,54] the potential energy surface corresponding to the 1^1B_u ionic state presents only one minimum. Its main geometric features are collected in Table 2. It shows an elongated transannular C–C bond (by 0.15 Å at SF-TD-DFT level) and a loss of planarity of the DHP core (by 16° at SF-TD-DFT level) relative to the ground-state structure. This minimum is

denoted CPD* in Figure 4, as it represents the first excited-state intermediate populated along the initial relaxation on the initially excited $S_2(1^1B_u)$ state with structural characteristics showing a clear distortion from DHP towards a CPD-like structure. The SF-TD-DFT CPD* structure lies somewhat in between the TD-DFT and CASSCF optimized geometries: while TD-DFT predicts a more DHP-like structure with a shorter transannular C–C bond and a more planar system, CASSCF tends to exaggerate the structural distortion towards CPD with a substantially longer transannular C–C bond and a more pronounced planarity loss. The MS-CASPT2 potential energy profiles in Figure 4 and in Figure S3 seem to support the position of this CPD* minimum to the SF-TD-DFT optimized structure rather than that of the CASSCF one. To be more precise, the MS-CASPT2 1^1B_u potential energy profile was computed along a LIIC path between the CPD* structures optimized at SF-TD-DFT and CASSCF levels (Figure S4 in SI). It confirms that the MS-CASPT2 CPD* minimum is expected to be closer to the SF-TD-DFT structure.

Table 2. Main geometrical parameters (see Scheme 1 for labeling definition) of ground-state DHP, excited-state 1^1B_u C_{2h} minimum structure (CPD*) and $S_2(1^1B_u)/S_1(1^1A_u)$ minimum energy conical intersection at various levels of theory.

Geometrical	DHP S_0 C_{2h} minimum			CPD* 1^1B_u C_{2h} minimum			$S_2(1^1B_u)/S_1(1^1A_u)$ MECI	
parameters[a]	SF-TD-DFT	DFT	CASSCF	SF-TD-DFT	TD-DFT	CASSCF	SF-TD-DFT	TD-DFT
a	1.389	1.399	1.400	1.389	1.403	1.396	1.387	1.403
b	1.382	1.392	1.392	1.380	1.389	1.387	1.380	1.390
c	1.395	1.400	1.400	1.431	1.433	1.433	1.434	1.430
d	1.381	1.395	1.396	1.360	1.375	1.368	1.356	1.377

q	1.510	1.520	1.541	1.662	1.615	1.782	1.717	1.604
ϕ	0.3	0.2	0.9	16.2	11.6	18.1	19.8	10.5

[a] Distances in angstroms and angles in degrees. q is the transannular C–C bond distance and ϕ is a dihedral angle measuring the planarity of the system.

The SF-TD-DFT potential energy profiles in Figure 4 shows that a crossing (conical intersection) occurs between the $S_2(1^1B_u)$ and $S_1(1^1A_u)$ state close to the $S_2(1^1B_u)$ CPD* minimum. This is in agreement with the MS-CASPT2 potential energy profiles (Figure 4) and previous CASPT2[54] and TD-DFT[36] studies. The $S_2(1^1B_u)$/ $S_1(1^1A_u)$ MECI optimized structure is reported in Table 2, which shows that it is indeed close to the $S_2(1^1B_u)$ CPD* minimum both at the SF-TD-DFT and TD-DFT levels. Moreover, it is energetically easily accessible, as it lies a mere 0.3 kcal/mol (0.014 eV) above CPD* at SF-TD-DFT level. Note that at the TD-DFT level, the MECI occurs before reaching the 1^1B_u CPD* minimum and lies only 0.03 kcal (0.001 eV) above it. This crossing plays thus the role of an efficient photophysical funnel, as it is responsible for the expected ultrafast depopulation of the photoisomerizing $S_2(1^1B_u)$ state towards the unreactive $S_1(1^1A_u)$ state (no photoisomerization is observed experimentally upon exciting directly this state[53]). The main difference between the SF-TD-DFT and MS-CASPT2 profiles is the position of this funnel, which occurs right at the CPD* minimum in MS-CASPT2. This is mainly the result of the energetic position of the $S_2(1^1B_u)$ state which is slightly too low at MS-CASPT2 level and slightly too high at SF-TD-DFT level compared to the highly accurate CC3 reference (see discussion above and Table 1).

The next interesting feature of these potential energy profiles is the presence of a near degeneracy between the 1^1B_u and the 2^1A_g excited states along the 1^1B_u relaxation pathway, both at the SF-TD-DFT and MS-CASPT2 levels. This near degeneracy occurs beyond the CPD*

minimum, requiring further geometrical distortion along the ring-opening reaction coordinate. As a consequence, it is interesting to investigate the relaxation pathway on the dark 2^1A_g excited state to determine if a possible deactivation channel is possible between these two states, as previously suggested in a CASPT2//CASSCF study (see Figure 2).[54]

It is also worth noting that the $S_3(2^1A_u)$ and $S_4(2^1B_u)$ states are not expected to play a role in the photoisomerization mechanism upon direct excitation to S_2, as their corresponding potential energy surfaces are not coupled with that of the 1^1B_u state along the 1^1B_u initial relaxation path.

4.3. Relaxation pathway along the dark 2^1A_g excited state. Figure 5 shows the SF-TD-DFT and MS-CASPT2 potential energy profiles along the relaxation path of the 2^1A_g state (see Figure S5 in SI for SF-TD-DFT profiles computed in the spin-unrestricted formulation). This relaxation path is approximated using the LIIC obtained by interpolating between the DHP ground-state minimum, the 2^1A_g excited-state minimum and the CPD ground-state minimum structures optimized at the SF-TD-DFT level. Figure S6 shows the MS-CASPT2 energy curves based on optimized CASSCF structures.

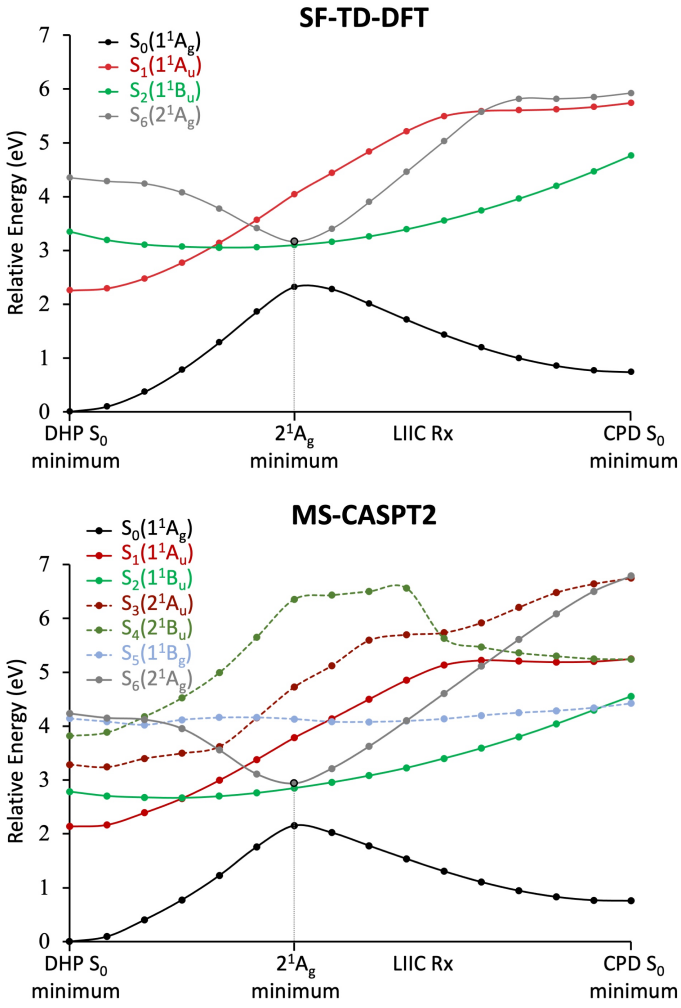

Figure 5. Potential energy profiles along the LIIC reaction path describing the approximate 2^1A_g relaxation pathway using SF-TD-DFT optimized structures. SF-TD-DFT results for the four relevant electronic states are shown (top) and MS-CASPT2 results for all states from S_0 to S_6 are shown (bottom). Dashed lines correspond to states not computed at SF-TD-DFT level. Color code based on symmetry labels.

The potential energy surface corresponding to the 2^1A_g covalent excited state presents also one minimum belonging to the C_{2h} symmetry. Its main geometric features are collected in Table 3. This minimum is the result of an avoided crossing with the 1^1A_g ground-state belonging to the same symmetry, as predicted by the state correlation diagram (cf. Figure 1b). Compared to the

CPD* 1^1B_u minimum structure, it is characterized by a further increase of the transannular bond length and of the distortion to planarity (Δq = +0.28 Å; $\Delta\phi$ = +8.8°). This structure is in good agreement with the CASSCF one. However, it is worth noting that at the CASSCF level, a second local minimum is found with a less distorted (more DHP-like) structure lying higher in energy (Table S1).[54] This minimum could not be found with SF-TD-DFT in the spin-restricted formulation (in contrast to the spin-unrestricted formulation; Figure S5) and the MS-CASPT2 profiles also corroborate the presence of only one minimum on the 2^1A_g potential energy surface with a strong distortion towards CPD formation. This minimum nearly coincides with a conical intersection between the 2^1A_g and 1^1B_u states, both at SF-TD-DFT and MS-CASPT2 levels (Figures 5, S5, S6). These states are now respectively lying on the S_2 and S_1 potential energy surfaces respectively, due to the various crossings with the other states along this relaxation pathway. The corresponding $S_2(2^1A_g)/S_1(1^1B_u)$ MECI optimized structure is almost indistinguishable from the 2^1A_g minimum structure (Table 3). It is located only 3.6 kcal/mol (0.155 eV) above the 1^1B_u CPD* minimum, suggesting the possibility of electronic population transfer from the ionic 1^1B_u to the covalent 2^1A_g excited state at this funnel, as suggested in a previous CASPT2//CASSCF study.[54] Note that this funnel cannot be optimized neither that the TD-DFT level (doubly-excited state nature of 2^1A_g), nor at the CASSCF level (ionic nature of 1^1B_u entailing strong dynamic electron correlation).

Table 3. Main geometrical parameters (see Scheme 1 for labeling definition) of excited-state 2^1A_g C_{2h} minimum structure and $S_2(2^1A_g)/S_1(1^1B_u)$ minimum energy conical intersection at various levels of theory.

Geometrical	2^1A_g C_{2h} minimum		$S_2(2^1A_g)/S_1(1^1B_u)$ C_{2h} MECI
parameters[a]	SF-TD-DFT	CASSCF	SF-TD-DFT

a	1.389	1.399	1.389
b	1.384	1.393	1.384
c	1.438	1.437	1.439
d	1.360	1.384	1.359
q	1.945	2.045	1.944
ϕ	25.0	23.0	25.2

[a] Distances in angstroms and angles in degrees. *q* is the transannular C–C bond distance and ϕ is a dihedral angle measuring the planarity of the system.

4.4. Relaxation pathway towards the photochemical funnel. Because of the presence of an avoided crossing between the ground 1^1A_g and the biradicaloid 2^1A_g states, one would expect to find a conical intersection between these two states upon breaking the C_{2h} symmetry due to the non-symmetrical interstate coupling. This crossing was first[54] identified for dimethyldihydropyrene at the CASSCF level as a S_0/S_1 MECI displaying a local triangular structure due to a three-electron/three-center bond CI, a well-known class of CI involving three weakly coupled electrons reminiscent of the one present in the H_3 molecule for all equilateral triangular geometries.[107] The CASSCF structure of this S_0/S_1 MECI is shown in Figure 6a. This MECI was assigned to a covalent/covalent state crossing correlating to the two ^1A_g states and playing the role of the photochemical funnel for the DHP to CPD photoisomerization. However, this MECI is located about 20 kcal/mol (0.87 eV) above the 2^1A_g excited-state minimum at the CASSCF(16,16)/cc-pVTZ level raising doubts on the accessibility to this funnel. Note that for dimethyldihydropyrene (**2c**), the MECI was located 12 kcal/mol above the 2^1A_g excited-state minimum at the CASSCF(12,12)/cc-pVDZ level.[54] In addition, the two degenerate S_0 and S_1 states split respectively by 18 kcal/mol (0.77 eV) and 17 kcal/mol (0.72 eV) at the MS-CASPT2 and SF-

TD-DFT levels at this geometry, showing the importance of differential electron dynamic correlation to describe this funnel accurately.

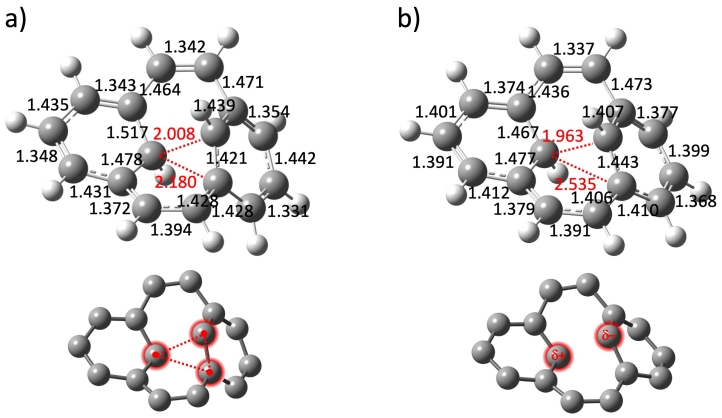

Figure 6. S_0/S_1 minimum energy conical intersection (MECI) optimized structures a) at the CASSCF level and b) at the SF-TD-DFT level. Illustration of the type of crossing involved (polyradical vs. zwitterionic).

The search of this photochemical funnel at the SF-TD-DFT level provided a rather different structure as shown in Figure 6b. While the CASSCF geometry presents an alternation of single and double bonds with a nearly isosceles triangular arrangement of the three carbon atoms bearing the weakly coupled electrons, the SF-TD-DFT structure breaks the local triangular picture but preserves the single/double bond alternation. The branching space spanned by the two first-order degeneracy-lifting coordinates, involves CC skeletal deformation as found at the CASSCF level, but also shows noticeable differences (see Figure S7 in SI). To elucidate the origin of this change in the MECI structure at the SF-TD-DFT level, it is important to determine the nature of the states involved at the crossing.

We first assumed that the S_0/S_1 MECI originates from the crossing between states correlating with the two ^1A_g states, as it is found at the CASSCF level. We thus considered the potential energy profiles along the approximate relaxation pathway between the 2^1A_g excited-state minimum and

the S_0/S_1 MECI (Figure 7). If we first consider the SF-TD-DFT profiles along the CASSCF pathway leading to the isosceles triangular MECI (Figure 7 top), they show that the gap between the states correlating with the two ^1A_g states increases, in complete contrast to what is observed at the CASSCF level (Figure S8 in SI). Rather, a crossing is found between the ground 1^1A_g state and the zwitterionic 1^1B_u state along this relaxation pathway. The same profiles but computed along the LIIC using the SF-TD-DFT optimized structures (Figure 7 bottom) confirms that the S_0/S_1 MECI found at the SF-TD-DFT level involves a crossing between the ground state and the zwitterionic excited state.

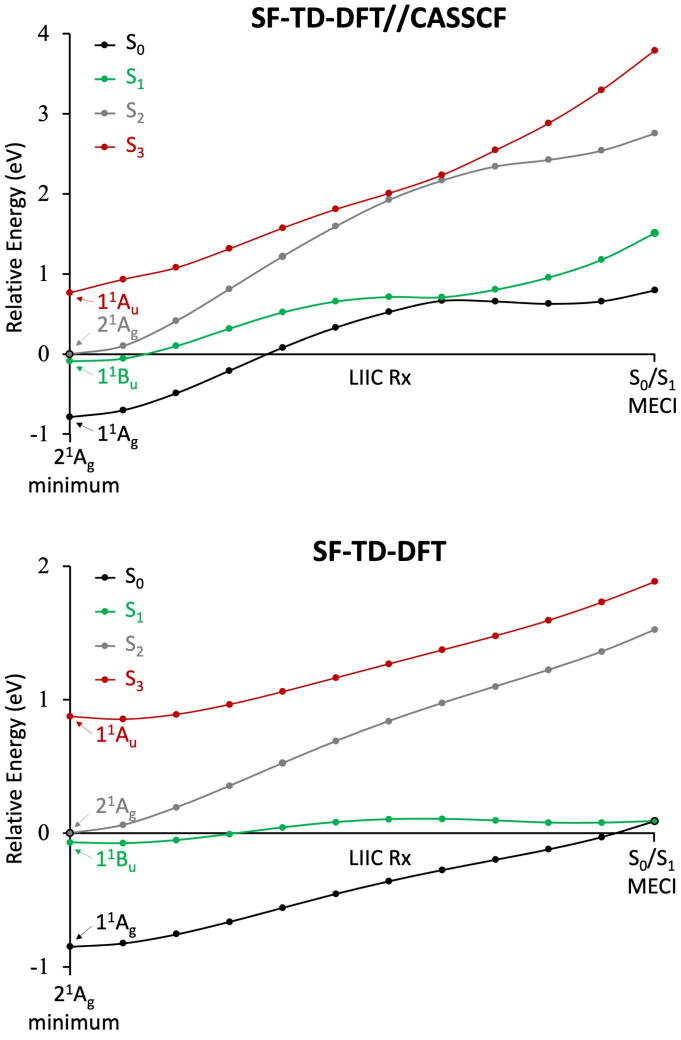

Figure 7. Potential energy profiles along the LIIC reaction path describing the approximate relaxation pathway from the 2^1A_g minimum to the S_0/S_1 MECI. SF-TD-DFT profiles along the CASSCF pathway (top) and SF-TD-DFT profiles along the SF-TD-DFT pathway (bottom). The four relevant electronic states are shown. Symmetry labeling strictly valid at the 2^1A_g C_{2h} minimum structure (first point on the extreme left of the profiles). Zero energy is set at the 2^1A_g minimum. S_n notation based on the actual state ordering. Color code based on adiabatic states.

Based on the above results, we can deduce that the 2^1A_g state does not need to be populated to access the photochemical funnel for the DHP→CPD isomerization. Rather, because the S_0/S_1 MECI involves the zwitterionic excited state, the system can directly access this funnel from population of the 1^1B_u state. The potential energy profiles for this pathway are shown in Figure 8 (see Figure S9 in SI for the profiles up to the CPD photoproduct at the SF and MR-SF levels). They show that the zwitterionic 1^1B_u state, after crossing the lower covalent 1^1A_u state (as already observed along the 1^1B_u symmetry-preserving relaxation path; cf. Figure 4 top), displays a potential energy barrier of ca. 12 kcal/mol (0.50 eV, providing an upper estimate based on the approximate LIIC path) before crossing the ground state. This S_0/S_1 MECI lies 5.7 kcal/mol (0.25 eV) above the 1^1B_u minimum, making the photochemical funnel energetically accessible in contrast to what is found at the CASSCF level. Note that for dimethyldihydropyrene (**2c**), this S_0/S_1 MECI is found 2.4 kcal/mol (0.10 eV) above the 1^1B_u minimum at the SF-TD-DFT level. The main electronic configurations for the four relevant states are also illustrated on Figure 8 at the 1^1B_u minimum and at S_0/S_1 MECI. They clearly show the configuration interchanges between the 1^1A_u and 1^1B_u states (crossing between red and green curves in Figure 8) but also between the 1^1A_u and 2^1A_g states (avoided crossing between green and gray curves in Figure 8). MS-RASPT2 calculations (as an approximation to MS-CASPT2, which is beyond our available computational

resources for calculations without symmetry) along this pathway bring further support to this mechanistic picture, as the corresponding potential energy profiles at this level of theory also show a narrowing of the energy gap between the ground and zwitterionic states towards the photochemical funnel (Figure S10 in SI). Note that the MR-SF-TD-DFT profiles (Figure S9 in SI) are also in very good agreement with the SF-TD-DFT ones, showing that spin-contamination only has a weak impact on the reliability of the potential energy profiles in this case.

It thus clearly appears that the three-electron/three-center bond conical intersection found at the CASSCF level and predicted by valence bond theory using only covalent configurations[107] is lost at the SF-TD-DFT and MS-CASPT2 levels due to the inclusion of low-energy ionic configurations missing at the CASSCF level. As a result, the photochemically relevant conical intersection changes nature from a polyradical to a zwitterionic type, as illustrated in Figure 6. This type of change in the nature of the photochemical funnel has been encountered before in dithienylethenes, although not explicitly described.[85,88]

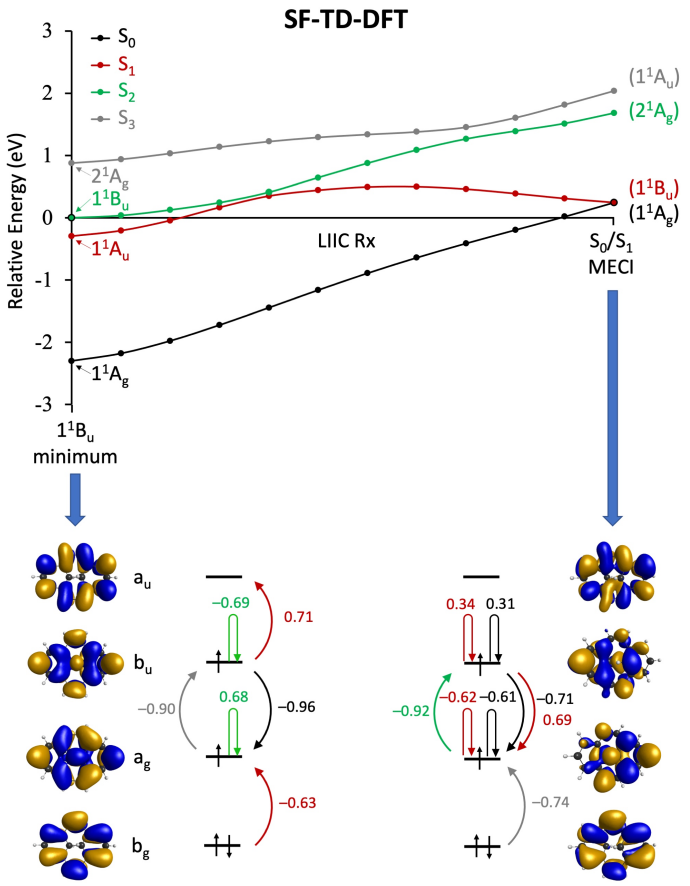

Figure 8. Potential energy profiles along the LIIC reaction path describing the approximate relaxation pathway from the 1^1B_u minimum to the S_0/S_1 MECI at the SF-TD-DFT level. The four relevant electronic states are shown. Symmetry labeling strictly valid at the 1^1B_u C_{2h} minimum structure (first point on the extreme left of the profiles). Zero energy is set at the 1^1B_u minimum. S_n notation based on the actual state ordering. Color code based on adiabatic states. Correlating states at the S_0/S_1 MECI geometry are shown in parentheses. SF-TD-DFT main configurations are shown at the 1^1B_u minimum and at the S_0/S_1 MECI geometries for all relevant states in the lower panel. The arrows and the associated numbers correspond to the one-electron spin-flip excitations with their transition amplitudes with the colors matching those of the corresponding adiabatic states.

5. CONCLUSION AND PERSPECTIVES

The DHP→CPD photoisomerization involves a coupled multi-state mechanism requiring a balanced treatment of the static and dynamic electron correlation along the excited-state reaction path due to the very different nature of the electronic states involved (covalent vs. ionic, singly- vs. doubly-excited). This study shows that SF-TD-DFT provides a powerful and efficient electronic structure method capable of describing the complex photoisomerization mechanism of this challenging photochromic system. Based on the present results, we are able to revise the photoisomerization mechanism formerly proposed on the basis of a CASPT2//CASSCF study for which the lack of dynamic electron correlation at the optimization step of the critical conical intersections was a main limitation. The new mechanistic picture is summarized in Figure 9, which is an updated scheme compared to the one shown in Figure 2. After photoexcitation to the bright zwitterionic $S_2(1^1B_u)$ state, the system relaxes on the corresponding potential energy surface to reach an intermediate denoted CPD* characterized by an elongated transannular C–C bond and a loss of planarity of the DHP core relative to the ground-state structure. In the vicinity of this excited-state minimum lies an easily accessible conical intersection with the lower non-photoisomerizing $S_1(1^1A_u)$ covalent excited state providing an efficient photophysical funnel at the origin of the low photoisomerization quantum yield of this system. To form the CPD photoproduct, the system needs to access the photochemical funnel which has been identified as an S_0/S_1 MECI involving the zwitterionic excited state. Whereas the ground-state potential energy barrier results from an avoided crossing with the doubly-excited state of the same symmetry (2^1A_g) as predicted by the correlation diagrams (Figure 1), SF-TD-DFT does not predict the involvement of this excited state in the photochemical path. The newly identified zwitterionic photochemical funnel is energetically accessible, unlike the three-electron/three-center bond funnel predicted at the

CASSCF level. Because of the much more available S_1/S_2 photophysical funnel, accessing the photochemical funnel region is expected to be a rare event for the unsubstituted DHP.

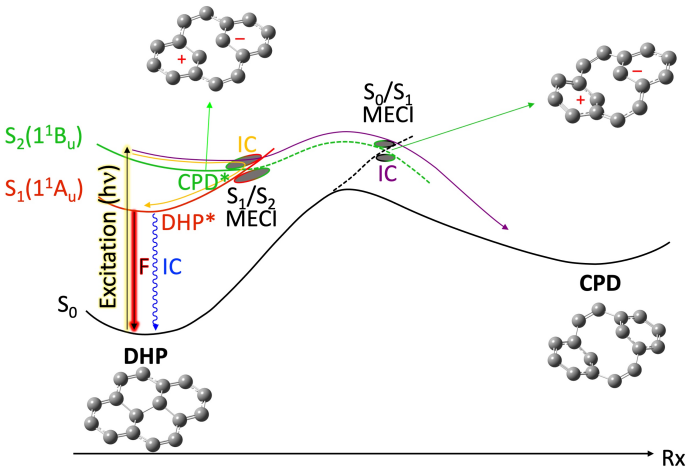

Figure 9. Revised schematic potential energy profiles of the relevant electronic states involved in the DHP/CPD photochromism based on SF-TD-DFT results. F: fluorescence, IC: internal conversion, MECI: minimum energy conical intersection. Relevant structures for which hydrogen atoms have been omitted for clarity are shown. Yellow curved arrow: photophysical pathway; purple curved arrow: photoisomerization (photochemical) pathway. Color code of the potential energy curves based on the diabatic nature of the electronic states. Full lines correspond to potential energy curves along C_{2h} symmetry-preserving coordinates and dashed lines to a symmetry-breaking coordinate.

This study further illustrates the importance of accurately describing differential electron correlation between electronic states of different character in the search of conical intersections and photochemical pathways. While CASSCF has undoubtedly been an outstanding tool to investigate photochemical processes involving conical intersections, this study shows that only correcting the energy at the second-order perturbation theory as most often done may not be sufficient to provide reliable photochemical paths if the dynamic electron correlation is not

included at the conical intersection optimization stage. Previous theoretical contributions have illustrated this point for the photoisomerization of smaller systems such as stilbene,[136] cis-diene[75,112] and retinal protonated Schiff base[77,137]. Several studies have shown recently how well SF-TD-DFT performs to optimize such critical funnel structures.[138,139,140] This method thus shows great promises to investigate the photochemistry of molecular systems for which state-of-the-art CASPT2 geometry optimizations of conical intersections are not achievable.

Future work should aim at investigating the DHP to CPD photoisomerization pathway beyond the static approach used herein. Quantum dynamics simulations using vibronic coupling theory have recently been performed to analyze the UV-Vis absorption properties of DHP and CPD.[141] On-the-fly mixed quantum-classical dynamics studies combined with femtosecond time-resolved spectroscopy would certainly shed new lights on the complex photoisomerization mechanism of DHP.

ASSOCIATED CONTENT

Supporting Information. The Supporting Information is available free of charge. Figures S1-S10 for complementary potential energy profiles computed at SF-TD-DFT, MR-SF-TD-DFT, MS-CASPT2, MS-RASPT2 and CASSCF levels and S_0/S_1 MECI branching space. Table S1 for optimized Cartesian coordinates (PDF).

AUTHOR INFORMATION

Corresponding Author

*Martial Boggio-Pasqua – Laboratoire de Chimie et Physique Quantiques, FeRMI, Université Paul Sabatier, CNRS, Université de Toulouse, 31062 Toulouse, France; E-mail: martial.boggio@irsamc.ups-tlse.fr

Author Contributions

E.L. performed all the calculations. R.S. contributed to the preliminary CASSCF and CASPT2 study. M.-C.H. contributed to discussions and improving the manuscript. M.B.-P. initiated the study, supervised the work and wrote the manuscript. All authors have given approval to the final version of the manuscript.

Notes

The authors declare no competing financial interest.

ACKNOWLEDGMENT

The authors thank the Agence Nationale de la Recherche through grant no. ANR-18-CE29-0012 (Photochromics project) and the EUR grant NanoX n°ANR-17-EURE-0009 for financial support. This work was granted access to the HPC resources of CALMIP supercomputing center under the allocation 2022-[12158]. We also thank the support team at CALMIP for installing GAMESS on the HPC center and David Sanchez for compilation of the Q-CHEM software on our local computing facilities.

ABBREVIATIONS

DHP, dihydropyrene; CPD, cyclophanediene; TD-DFT, time-dependent density functional theory; SF-TD-DFT, spin-flip time-dependent density functional theory; MECI, minimum energy conical intersection. CASSCF, complete active space self-consistent field; CASPT2,

complete active space second-order perturbation theory; MS-CASPT2, multistate complete active space second-order perturbation theory; MS-RASPT2, multistate restricted active space second-order perturbation theory; CC3, coupled cluster singles, doubles and perturbative triples; VTE, vertical transition energy; HOMO, highest occupied molecular orbital; LUMO, lowest unoccupied molecular orbital. LIIC, linearly-interpolated in internal coordinates; FC, Franck-Condon.

REFERENCES

(1) Irie, M. Diarylethenes for Memories and Switches. *Chem. Rev.* **2000**, *100* (5), 1685–1716. https://doi.org/10.1021/cr980069d.

(2) Yokoyama, Y. Fulgides for Memories and Switches. *Chem. Rev.* **2000**, *100* (5), 1717–1740. https://doi.org/10.1021/cr980070c.

(3) Berkovic, G.; Krongauz, V.; Weiss, V. Spiropyrans and Spirooxazines for Memories and Switches. *Chem. Rev.* **2000**, *100* (5), 1741–1754. https://doi.org/10.1021/cr9800715.

(4) Szaciłowski, K. Digital Information Processing in Molecular Systems. *Chem. Rev.* **2008**, *108* (9), 3481–3548. https://doi.org/10.1021/cr068403q.

(5) Russew, M.-M.; Hecht, S. Photoswitches: From Molecules to Materials. *ADVANCED MATERIALS*, 2010, *22*, 3348–3360. https://doi.org/10.1002/adma.200904102.

(6) Szymański, W.; Beierle, J. M.; Kistemaker, H. A. V.; Velema, W. A.; Feringa, B. L. Reversible Photocontrol of Biological Systems by the Incorporation of Molecular Photoswitches. *Chem. Rev.* **2013**, *113* (8), 6114–6178. https://doi.org/10.1021/cr300179f.

(7) Asadirad, A. M.; Boutault, S.; Erno, Z.; Branda, N. R. Controlling a Polymer Adhesive Using Light and a Molecular Switch. *J. Am. Chem. Soc.* **2014**, *136* (8), 3024–3027. https://doi.org/10.1021/ja500496n.

(8) Kim, T.; Zhu, L.; Al-Kaysi, R. O.; Bardeen, C. J. Organic Photomechanical Materials. *CHEMPHYSCHEM*, 2014, *15*, 400–414. https://doi.org/10.1002/cphc.201300906.

(9) Tochitsky, I.; Kienzler, M. A.; Isacoff, E.; Kramer, R. H. Restoring Vision to the Blind with Chemical Photoswitches. *Chemical Reviews* **2018**, *118* (21), 10748–10773. https://doi.org/10.1021/acs.chemrev.7b00723.

(10) Yu, Q.; Aguila, B.; Gao, J.; Xu, P.; Chen, Q.; Yan, J.; Xing, D.; Chen, Y.; Cheng, P.; Zhang, Z.; Ma, S. Photomechanical Organic Crystals as Smart Materials for Advanced Applications. *CHEMISTRY-A EUROPEAN JOURNAL*, 2019, *25*, 5611–5622. https://doi.org/10.1002/chem.201805382.

(11) Boelke, J.; Hecht, S. Designing Molecular Photoswitches for Soft Materials Applications. *ADVANCED OPTICAL MATERIALS*, 2019, *7*. https://doi.org/10.1002/adom.201900404.

(12) Pianowski, Z. L. Recent Implementations of Molecular Photoswitches into Smart Materials and Biological Systems. *Chemistry – A European Journal* **2019**, *25* (20), 5128–5144. https://doi.org/10.1002/chem.201805814.

(13) Goulet-Hanssens, A.; Eisenreich, F.; Hecht, S. Enlightening Materials with Photoswitches. *Adv. Mater.* **2020**, *32* (20), 1905966. https://doi.org/10.1002/adma.201905966.

(14) Dürr, H.; Bouas-Laurent, H. *Photochromism: Molecules and Systems*, Elsevier.; Amsterdam, 2003.

(15) Crano, J. C.; Guglielmetti, R. J. *Organic Photochromic and Thermochromic Compounds*, Springer.; New York, 2002.

(16) Feringa, B. L.; Browne, W. R. *Molecular Switches*, Wiley-VCH Verlag GmbH&Co. KGaA.; Weinheim, Germany, 2011.

(17) Mitchell, R. H. The Metacyclophanediene-Dihydropyrene Photochromic π Switch. *European Journal of Organic Chemistry* **1999**, *1999* (11), 2695–2703. https://doi.org/10.1002/(SICI)1099-0690(199911)1999:11<2695::AID-EJOC2695>3.0.CO;2-T.

(18) Roldan, D.; Kaliginedi, V.; Cobo, S.; Kolivoska, V.; Bucher, C.; Hong, W.; Royal, G.; Wandlowski, T. Charge Transport in Photoswitchable Dimethyldihydropyrene-Type Single-Molecule Junctions. *Journal of the American Chemical Society* **2013**, *135* (16), 5974–5977. https://doi.org/10.1021/ja401484j.

(19) Tsuji, Y.; Hoffmann, R. Frontier Orbital Control of Molecular Conductance and Its Switching. *Angewandte Chemie* **2014**, *126* (16), 4177–4181. https://doi.org/10.1002/ange.201311134.

(20) Bakkar, A.; Lafolet, F.; Roldan, D.; Puyoo, E.; Jouvenot, D.; Royal, G.; Saint-Aman, E.; Cobo, S. Bidirectional Light-Induced Conductance Switching in Molecular Wires Containing a Dimethyldihydropyrene Unit. *Nanoscale* **2018**, *10* (12), 5436–5441. https://doi.org/10.1039/C7NR09551A.

(21) Zhang, G.-P.; Mu, Y.-Q.; Zhao, J.-M.; Huang, H.; Hu, G.-C.; Li, Z.-L.; Wang, C.-K. Optimizing the Conductance Switching Performance in Photoswitchable Dimethyldihydropyrene/Cyclophanediene Single-Molecule Junctions. *Physica E: Low-dimensional Systems and Nanostructures* **2019**, *109*, 1–5. https://doi.org/10.1016/j.physe.2018.12.032.

(22) Mu, Y.-Q.; Zhao, J.-M.; Chen, L.-Y.; Huang, H.; Wang, M.-L.; Hu, G.-C.; Wang, C.-K.; Zhang, G.-P. Odd-Even Effect of the Switching Performance for Dimethyldihydropyrene/Cyclophanediene Single-Molecule Switch Modulated by Carbon Atomic Chains. *Organic Electronics* **2020**, *81*, 105665. https://doi.org/10.1016/j.orgel.2020.105665.

(23) Ghosh, S.; Hossain, M. S.; Chatterjee, S.; Rahaman, Sk. A.; Bandyopadhyay, S. Light-Gated Modulation of Electronic Mobility of a Dihydropyrene-Based Photochromic Coordination

Polymer. *ACS Appl. Mater. Interfaces* **2020**, *12* (47), 52983–52991. https://doi.org/10.1021/acsami.0c17513.

(24) Huang, X.; Li, T. Recent Progress in the Development of Molecular-Scale Electronics Based on Photoswitchable Molecules. *J. Mater. Chem. C* **2020**, *8* (3), 821–848. https://doi.org/10.1039/C9TC06054E.

(25) Blattmann, H.-R.; Meuche, D.; Heilbronner, E.; Molyneux, R. J.; Boekelheide, V. Photoisomerization of Trans-15,16-Dimethyldihydropyrene. *J. Am. Chem. Soc.* **1965**, *87* (1), 130–131. https://doi.org/10.1021/ja01079a031.

(26) Boekelheide, V.; Miyasaka, T. Aromatic Molecules Bearing Substituents within the Cavity of the π-Electron Cloud. Synthesis of Trans-15,16-Diethyldihydropyrene. *Journal of the American Chemical Society* **1967**, 6.

(27) Murphy, R. S.; Chen, Y.; Ward, T. R.; Mitchell, R. H.; Bohne, C. Photophysical Studies on the Photochromism of Trans-10b,10c-Dimethyldihydropyrene. *Chemical Communications* **1999**, 2097–2098.

(28) Mitchell, R. H.; Iyer, V. S.; Mahadevan, R.; Venugopalan, S.; Zhou, P. Annelated Dimethyldihydropyrenes. Electrophilic Substitution and Valence Isomerization to Metacyclophanedienes. *The Journal of Organic Chemistry* **1996**, *61* (15), 5116–5120. https://doi.org/10.1021/jo9601573.

(29) Sheepwash, M. A. L.; Mitchell, R. H.; Bohne, C. Mechanistic Insights into the Photochromism of Trans-10b,10c-Dimethyl-10b,10c-Dihydropyrene Derivatives. *Journal of the American Chemical Society* **2002**, *124* (17), 4693–4700. https://doi.org/10.1021/ja017229e.

(30) Sheepwash, M. A. L.; Ward, T. R.; Wang, Y.; Bandyopadhyay, S.; Mitchell, R. H.; Bohne, C. Mechanistic Studies on the Photochromism of [e]-Annelated Dimethyldihydropyrenes. *Photochem. Photobiol. Sci.* **2003**, *2* (2), 104–112. https://doi.org/10.1039/B208952A.

(31) Williams, R. V.; Edwards, W. D.; Mitchell, R. H.; Robinson, S. G. A DFT Study of the Thermal, Orbital Symmetry Forbidden, Cyclophanediene to Dihydropyrene Electrocyclic Reaction. Predictions to Improve the Dimethyldihydropyrene Photoswitches. *Journal of the American Chemical Society* **2005**, *127* (46), 16207–16214. https://doi.org/10.1021/ja054553r.

(32) Mitchell, R. H.; Bohne, C.; Robinson, S. G.; Yang, Y. The Effect of Addition of Fluorescent Moieties to Dihydropyrenes: Enhancing Photochromicity and Fluorescence Monitoring. *The Journal of Organic Chemistry* **2007**, *72* (21), 7939–7946. https://doi.org/10.1021/jo0712392.

(33) Ayub, K.; Li, R.; Bohne, C.; Williams, R. V.; Mitchell, R. H. Calculation Driven Synthesis of an Excellent Dihydropyrene Negative Photochrome and Its Photochemical Properties. *Journal of the American Chemical Society* **2011**, *133* (11), 4040–4045. https://doi.org/10.1021/ja1100596.

(34) Khan, N.; Sheikh, N. S.; Khan, A. F.; Ludwig, R.; Mahmood, T.; Rehman, W.; Al-Faiyz, Y. S. S.; Ayub, K. Towards Thermally Stable Cyclophanediene-Dihydropyrene Photoswitches. *J Mol Model* **2015**, *21* (6), 1–11. https://doi.org/10.1007/s00894-015-2695-0.

(35) Roldan, D.; Cobo, S.; Lafolet, F.; Vilà, N.; Bochot, C.; Bucher, C.; Saint-Aman, E.; Boggio-Pasqua, M.; Garavelli, M.; Royal, G. A Multi-Addressable Switch Based on the Dimethyldihydropyrene Photochrome with Remarkable Proton-Triggered Photo-Opening Efficiency. *Chemistry – A European Journal* **2015**, *21* (1), 455–467. https://doi.org/10.1002/chem.201404858.

(36) Boggio-Pasqua, M.; Garavelli, M. Rationalization and Design of Enhanced Photoinduced Cycloreversion in Photochromic Dimethyldihydropyrenes by Theoretical Calculations. *The Journal of Physical Chemistry A* **2015**, *119* (23), 6024–6032. https://doi.org/10.1021/jp5118773.

(37) Mitchell, R. H.; Ward, T. R.; Wang, Y.; Dibble, P. W. Pi-Switches: Synthesis of Three-Way Molecular Switches Based on the Dimethyldihydropyrene−Metacyclophanediene Valence Isomerization. *J. Am. Chem. Soc.* **1999**, *121* (11), 2601–2602. https://doi.org/10.1021/ja983848k.

(38) Mitchell, R. H.; Bohne, C.; Wang, Y.; Bandyopadhyay, S.; Wozniak, C. B. Multistate π Switches: Synthesis and Photochemistry of a Molecule Containing Three Switchable Annelated Dihydropyrene Units. *The Journal of Organic Chemistry* **2006**, *71* (1), 327–336. https://doi.org/10.1021/jo052153g.

(39) Muratsugu, S.; Kume, S.; Nishihara, H. Redox-Assisted Ring Closing Reaction of the Photogenerated Cyclophanediene Form of Bis(Ferrocenyl)Dimethyldihydropyrene with Interferrocene Electronic Communication Switching. *Journal of the American Chemical Society* **2008**, *130* (23), 7204–7205. https://doi.org/10.1021/ja8016494.

(40) Muratsugu, S.; Kishida, M.; Sakamoto, R.; Nishihara, H. Comparative Study of Photochromic Ferrocene-Conjugated Dimethyldihydropyrene Derivatives. *Chem. Eur. J.* **2013**, *19* (51), 17314–17327. https://doi.org/10.1002/chem.201303456.

(41) Vilà, N.; Royal, G.; Loiseau, F.; Deronzier, A. Photochromic and Redox Properties of Bisterpyridine Ruthenium Complexes Based on Dimethyldihydropyrene Units as Bridging Ligands. *Inorganic Chemistry* **2011**, *50* (21), 10581–10591. https://doi.org/10.1021/ic2003904.

(42) Muratsugu, S.; Nishihara, H. π-Conjugation Modification of Photochromic and Redox-Active Dimethyldihydropyrene by Phenyl- and Ethynyl-Terpyridines and Ru(Bis-Terpyridine) Complexes. *New J. Chem.* **2014**, *38* (12), 6114–6124. https://doi.org/10.1039/C4NJ01462F.

(43) Bakkar, A.; Cobo, S.; Lafolet, F.; Roldan, D.; Saint-Aman, E.; Royal, G. A Redox- and Photo-Responsive Quadri-State Switch Based on Dimethyldihydropyrene-Appended Cobalt Complexes. *Journal of Materials Chemistry C* **2016**, *4* (6), 1139–1143. https://doi.org/10.1039/C5TC04277A.

(44) Bakkar, A.; Cobo, S.; Lafolet, F.; Boggio-Pasqua, M.; Royal, G.; Saint Aman, E. Self-Assembled Dimethyldihydropyrene-Pyridyl Substituted Ligands with Zinc(II) Meso-Tetraphenylporphyrin via Axial Coordination. *Dalton Transactions* **2016**, *45* (41), 16453–16462. https://doi.org/10.1039/C6DT02975B.

(45) Jacquet, M.; Lafolet, F.; Cobo, S.; Loiseau, F.; Bakkar, A.; Boggio-Pasqua, M.; Saint-Aman, E.; Royal, G. Efficient Photoswitch System Combining a Dimethyldihydropyrene Pyridinium Core and Ruthenium(II) Bis-Terpyridine Entities. *Inorganic Chemistry* **2017**, *56* (8),

4357–4368. https://doi.org/10.1021/acs.inorgchem.6b02861.

(46) Jacquet, M.; Uriarte, L. M.; Lafolet, F.; Boggio-Pasqua, M.; Sliwa, M.; Loiseau, F.; Saint-Aman, E.; Cobo, S.; Royal, G. All Visible Light Switch Based on the Dimethyldihydropyrene Photochromic Core. *J. Phys. Chem. Lett.* **2020**, 7.

(47) Straight, S. D.; Andréasson, J.; Kodis, G.; Bandyopadhyay, S.; Mitchell, R. H.; Moore, T. A.; Moore, A. L.; Gust, D. Molecular AND and INHIBIT Gates Based on Control of Porphyrin Fluorescence by Photochromes. *Journal of the American Chemical Society* **2005**, *127* (26), 9403–9409. https://doi.org/10.1021/ja051218u.

(48) Klaue, K.; Garmshausen, Y.; Hecht, S. Taking Photochromism beyond Visible: Direct One-Photon NIR Photoswitches Operating in the Biological Window. *Angewandte Chemie International Edition* **2018**, *57* (5), 1414–1417. https://doi.org/10.1002/anie.201709554.

(49) Klaue, K.; Han, W.; Liesfeld, P.; Berger, F.; Garmshausen, Y.; Hecht, S. Donor–Acceptor Dihydropyrenes Switchable with Near-Infrared Light. *J. Am. Chem. Soc.* **2020**, *142* (27), 11857–11864. https://doi.org/10.1021/jacs.0c04219.

(50) Ziani, Z.; Cobo, S.; Loiseau, F.; Jouvenot, D.; Lognon, E.; Boggio-Pasqua, M.; Royal, G. All Visible Light Photoswitch Based on the Dimethyldihydropyrene Unit Operating in Aqueous Solutions with High Quantum Yields. *JACS Au* **2023**, *3* (1), 131–142. https://doi.org/10.1021/jacsau.2c00552.

(51) Cobo, S.; Lafolet, F.; Saint-Aman, E.; Philouze, C.; Bucher, C.; Silvi, S.; Credi, A.; Royal, G. Reactivity of a Pyridinium-Substituted Dimethyldihydropyrene Switch under Aerobic Conditions: Self-Sensitized Photo-Oxygenation and Thermal Release of Singlet Oxygen. *Chemical Communications* **2015**, *51* (73), 13886–13889. https://doi.org/10.1039/C5CC04763C.

(52) Boggio-Pasqua, M.; López Vidal, M.; Garavelli, M. Theoretical Mechanistic Study of Self-Sensitized Photo-Oxygenation and Singlet Oxygen Thermal Release in a Dimethyldihydropyrene Derivative. *Journal of Photochemistry and Photobiology A: Chemistry* **2017**, *333*, 156–164. https://doi.org/10.1016/j.jphotochem.2016.10.020.

(53) Ziani, Z.; Loiseau, F.; Lognon, E.; Boggio-Pasqua, M.; Philouze, C.; Cobo, S.; Royal, G. Synthesis of a Negative Photochrome with High Switching Quantum Yields and Capable of Singlet-Oxygen Production and Storage. *Chemistry – A European Journal* **2021**, *27* (67), 16642–16653. https://doi.org/10.1002/chem.202103003.

(54) Boggio-Pasqua, M.; Bearpark, M. J.; Robb, M. A. Toward a Mechanistic Understanding of the Photochromism of Dimethyldihydropyrenes. *The Journal of Organic Chemistry* **2007**, *72* (12), 4497–4503. https://doi.org/10.1021/jo070452v.

(54) Sarkar, R.; Heitz, M.-C.; Royal, G.; Boggio-Pasqua, M. Electronic Excited States and UV–Vis Absorption Spectra of the Dihydropyrene/Cyclophanediene Photochromic Couple: A Theoretical Investigation. *J. Phys. Chem. A* **2020**, *124* (8), 1567–1579. https://doi.org/10.1021/acs.jpca.9b11262.

(56) Andersson, Kerstin.; Malmqvist, P. Aake.; Roos, B. O.; Sadlej, A. J.; Wolinski, Krzysztof.

Second-Order Perturbation Theory with a CASSCF Reference Function. *J. Phys. Chem.* **1990**, *94* (14), 5483–5488. https://doi.org/10.1021/j100377a012.

(57) Andersson, K.; Malmqvist, P.; Roos, B. O. Second-order Perturbation Theory with a Complete Active Space Self-consistent Field Reference Function. *J. Chem. Phys.* **1992**, *96* (2), 1218–1226. https://doi.org/10.1063/1.462209.

(58) Finley, J.; Malmqvist, P.-Å.; Roos, B. O.; Serrano-Andrés, L. The Multi-State CASPT2 Method. *Chemical Physics Letters* **1998**, *288* (2–4), 299–306. https://doi.org/10.1016/S0009-2614(98)00252-8.

(59) Roca-Sanjuán, D.; Aquilante, F.; Lindh, R. Multiconfiguration Second-Order Perturbation Theory Approach to Strong Electron Correlation in Chemistry and Photochemistry. *Wiley Interdisciplinary Reviews: Computational Molecular Science* **2012**, *2* (4), 585–603. https://doi.org/10.1002/wcms.97.

(60) Roos, O.; Andersson, K. Multiconfigurational Perturbation Theory with Level Shift - the Cr_2 Potential Revisited. *Chemical Physics Letters* **1995**, 9.

(61) Forsberg, N.; Malmqvist, P.-Å. Multiconfiguration Perturbation Theory with Imaginary Level Shift. *Chemical Physics Letters* **1997**, *274* (1–3), 196–204. https://doi.org/10.1016/S0009-2614(97)00669-6.

(62) Ghigo, G.; Roos, B. O.; Malmqvist, P.-Å. A Modified Definition of the Zeroth-Order Hamiltonian in Multiconfigurational Perturbation Theory (CASPT2). *Chemical Physics Letters* **2004**, *396* (1–3), 142–149. https://doi.org/10.1016/j.cplett.2004.08.032.

(63) Celani, P.; Werner, H.-J. Multireference Perturbation Theory for Large Restricted and Selected Active Space Reference Wave Functions. *The Journal of Chemical Physics* **2000**, *112* (13), 5546–5557. https://doi.org/10.1063/1.481132.

(64) Aquilante, F.; Malmqvist, P.-Å.; Pedersen, T. B.; Ghosh, A.; Roos, B. O. Cholesky Decomposition-Based Multiconfiguration Second-Order Perturbation Theory (CD-CASPT2): Application to the Spin-State Energetics of Co^{III}(Diiminato)(NPh). *J. Chem. Theory Comput.* **2008**, *4* (5), 694–702. https://doi.org/10.1021/ct700263h.

(65) Aquilante, F.; Todorova, T. K.; Gagliardi, L.; Pedersen, T. B.; Roos, B. O. Systematic Truncation of the Virtual Space in Multiconfigurational Perturbation Theory. *The Journal of Chemical Physics* **2009**, *131* (3), 034113. https://doi.org/10.1063/1.3157463.

(66) Yanai, T.; Saitow, M.; Xiong, X.-G.; Chalupský, J.; Kurashige, Y.; Guo, S.; Sharma, S. Multistate Complete-Active-Space Second-Order Perturbation Theory Based on Density Matrix Renormalization Group Reference States. *J. Chem. Theory Comput.* **2017**, *13* (10), 4829–4840. https://doi.org/10.1021/acs.jctc.7b00735.

(67) Celani, P.; Werner, H.-J. Analytical Energy Gradients for Internally Contracted Second-Order Multireference Perturbation Theory. *The Journal of Chemical Physics* **2003**, *119* (10), 5044–5057. https://doi.org/10.1063/1.1597672.

(68) Shiozaki, T.; Győrffy, W.; Celani, P.; Werner, H.-J. Communication: Extended Multi-State

Complete Active Space Second-Order Perturbation Theory: Energy and Nuclear Gradients. *The Journal of Chemical Physics* **2011**, *135* (8), 081106. https://doi.org/10.1063/1.3633329.

(69) Győrffy, W.; Shiozaki, T.; Knizia, G.; Werner, H.-J. Analytical Energy Gradients for Second-Order Multireference Perturbation Theory Using Density Fitting. *The Journal of Chemical Physics* **2013**, *138* (10), 104104. https://doi.org/10.1063/1.4793737.

(70) MacLeod, M. K.; Shiozaki, T. Communication: Automatic Code Generation Enables Nuclear Gradient Computations for Fully Internally Contracted Multireference Theory. *The Journal of Chemical Physics* **2015**, *142* (5), 051103. https://doi.org/10.1063/1.4907717.

(71) Vlaisavljevich, B.; Shiozaki, T. Nuclear Energy Gradients for Internally Contracted Complete Active Space Second-Order Perturbation Theory: Multistate Extensions. *J. Chem. Theory Comput.* **2016**, *12* (8), 3781–3787. https://doi.org/10.1021/acs.jctc.6b00572.

(72) Park, J. W.; Al-Saadon, R.; Strand, N. E.; Shiozaki, T. Imaginary Shift in CASPT2 Nuclear Gradient and Derivative Coupling Theory. *J. Chem. Theory Comput.* **2019**, *15* (7), 4088–4098. https://doi.org/10.1021/acs.jctc.9b00368.

(73) Park, J. W.; Shiozaki, T. Analytical Derivative Coupling for Multistate CASPT2 Theory. *J. Chem. Theory Comput.* **2017**, *13* (6), 2561–2570. https://doi.org/10.1021/acs.jctc.7b00018.

(74) Levine, B. G.; Coe, J. D.; Martínez, T. J. Optimizing Conical Intersections without Derivative Coupling Vectors: Application to Multistate Multireference Second-Order Perturbation Theory (MS-CASPT2) †. *J. Phys. Chem. B* **2008**, *112* (2), 405–413. https://doi.org/10.1021/jp0761618.

(75) Mori, T.; Kato, S. Dynamic Electron Correlation Effect on Conical Intersections in Photochemical Ring-Opening Reaction of Cyclohexadiene: MS-CASPT2 Study. *Chemical Physics Letters* **2009**, *476* (1–3), 97–100. https://doi.org/10.1016/j.cplett.2009.05.067.

(76) Park, J. W. Single-State Single-Reference and Multistate Multireference Zeroth-Order Hamiltonians in MS-CASPT2 and Conical Intersections. *J. Chem. Theory Comput.* **2019**, *15* (7), 3960–3973. https://doi.org/10.1021/acs.jctc.9b00067.

(77) Liu, L.; Liu, J.; Martinez, T. J. Dynamical Correlation Effects on Photoisomerization: Ab Initio Multiple Spawning Dynamics with MS-CASPT2 for a Model *Trans* -Protonated Schiff Base. *J. Phys. Chem. B* **2016**, *120* (8), 1940–1949. https://doi.org/10.1021/acs.jpcb.5b09838.

(78) Park, J. W.; Shiozaki, T. On-the-Fly CASPT2 Surface-Hopping Dynamics. *Journal of Chemical Theory and Computation* **2017**, *13* (8), 3676–3683. https://doi.org/10.1021/acs.jctc.7b00559.

(79) Park, J. W.; Al-Saadon, R.; MacLeod, M. K.; Shiozaki, T.; Vlaisavljevich, B. Multireference Electron Correlation Methods: Journeys along Potential Energy Surfaces. *Chem. Rev.* **2020**, *120* (13), 5878–5909. https://doi.org/10.1021/acs.chemrev.9b00496.

(80) Shao, Y.; Head-Gordon, M.; Krylov, A. I. The Spin–Flip Approach within Time-Dependent Density Functional Theory: Theory and Applications to Diradicals. *The Journal of Chemical Physics* **2003**, *118* (11), 4807–4818. https://doi.org/10.1063/1.1545679.

(81) Zhang, X.; Herbert, J. M. Analytic Derivative Couplings for Spin-Flip Configuration Interaction Singles and Spin-Flip Time-Dependent Density Functional Theory. *The Journal of Chemical Physics* **2014**, *141* (6), 064104. https://doi.org/10.1063/1.4891984.

(82) Minezawa, N.; Gordon, M. S. Optimizing Conical Intersections by Spin−Flip Density Functional Theory: Application to Ethylene. *J. Phys. Chem. A* **2009**, *113* (46), 12749–12753. https://doi.org/10.1021/jp908032x.

(83) Huix-Rotllant, M.; Natarajan, B.; Ipatov, A.; Muhavini Wawire, C.; Deutsch, T.; Casida, M. E. Assessment of Noncollinear Spin-Flip Tamm–Dancoff Approximation Time-Dependent Density-Functional Theory for the Photochemical Ring-Opening of Oxirane. *Physical Chemistry Chemical Physics* **2010**, *12* (39), 12811. https://doi.org/10.1039/c0cp00273a.

(84) Xu, X.; Gozem, S.; Olivucci, M.; Truhlar, D. G. Combined Self-Consistent-Field and Spin-Flip Tamm–Dancoff Density Functional Approach to Potential Energy Surfaces for Photochemistry. *J. Phys. Chem. Lett.* **2013**, *4* (2), 253–258. https://doi.org/10.1021/jz301935x.

(85) Isegawa, M.; Morokuma, K. Photochemical Ring Opening and Closing of Three Isomers of Diarylethene: Spin–Flip Time-Dependent Density Functional Study. *The Journal of Physical Chemistry A* **2015**, *119* (18), 4191–4199. https://doi.org/10.1021/jp511474f.

(86) Li, Y.; Liu, F.; Wang, B.; Su, Q.; Wang, W.; Morokuma, K. Different Conical Intersections Control Nonadiabatic Photochemistry of Fluorene Light-Driven Molecular Rotary Motor: A CASSCF and Spin-Flip DFT Study. *J. Chem. Phys.* **2016**, *145* (24), 244311. https://doi.org/10.1063/1.4972825.

(87) Salazar, E.; Faraji, S. Theoretical Study of Cyclohexadiene/Hexatriene Photochemical Interconversion Using Spin-Flip Time-Dependent Density Functional Theory. *Molecular Physics* **2020**, e1764120. https://doi.org/10.1080/00268976.2020.1764120.

(88) Salazar, E.; Reinink, S.; Faraji, S. Providing Theoretical Insight into the Role of Symmetry in the Photoisomerization Mechanism of a Non-Symmetric Dithienylethene Photoswitch. *Phys. Chem. Chem. Phys.* **2022**, *24* (19), 11592–11602. https://doi.org/10.1039/D2CP00550F.

(88) Harabuchi, Y.; Keipert, K.; Zahariev, F.; Taketsugu, T.; Gordon, M. S. Dynamics Simulations with Spin-Flip Time-Dependent Density Functional Theory: Photoisomerization and Photocyclization Mechanisms of *Cis*-Stilbene in ππ* States. *The Journal of Physical Chemistry A* **2014**, *118* (51), 11987–11998. https://doi.org/10.1021/jp5072428.

(90) Zhang, X.; Herbert, J. M. Spin-Flip, Tensor Equation-of-Motion Configuration Interaction with a Density-Functional Correction: A Spin-Complete Method for Exploring Excited-State Potential Energy Surfaces. *The Journal of Chemical Physics* **2015**, *143* (23), 234107. https://doi.org/10.1063/1.4937571.

(90) Yue, L.; Liu, Y.; Zhu, C. Performance of TDDFT with and without Spin-Flip in Trajectory Surface Hopping Dynamics: *Cis–Trans* Azobenzene Photoisomerization. *Physical Chemistry Chemical Physics* **2018**, *20* (37), 24123–24139. https://doi.org/10.1039/C8CP03851A.

(92) Minezawa, N.; Nakajima, T. Trajectory Surface Hopping Molecular Dynamics Simulation

by Spin-Flip Time-Dependent Density Functional Theory. *The Journal of Chemical Physics* **2019**, *150* (20), 204120. https://doi.org/10.1063/1.5096217.

(93) Minezawa, N.; Nakajima, T. Quantum Mechanical/Molecular Mechanical Trajectory Surface Hopping Molecular Dynamics Simulation by Spin-Flip Time-Dependent Density Functional Theory. *J. Chem. Phys.* **2020**, *152* (2), 024119. https://doi.org/10.1063/1.5132879.

(94) Uratani, H.; Morioka, T.; Yoshikawa, T.; Nakai, H. Fast Nonadiabatic Molecular Dynamics via Spin-Flip Time-Dependent Density-Functional Tight-Binding Approach: Application to Nonradiative Relaxation of Tetraphenylethylene with Locked Aromatic Rings. *Journal of Chemical Theory and Computation* **2020**. https://doi.org/10.1021/acs.jctc.0c00936.

(95) Uratani, H.; Yoshikawa, T.; Nakai, H. Trajectory Surface Hopping Approach to Condensed-Phase Nonradiative Relaxation Dynamics Using Divide-and-Conquer Spin-Flip Time-Dependent Density-Functional Tight Binding. *J. Chem. Theory Comput.* **2021**, *17* (3), 1290–1300. https://doi.org/10.1021/acs.jctc.0c01155.

(96) Longuet-Higgins, H. C.; Abrahamson, E. W. The Electronic Mechanism of Electrocyclic Reactions. *J. Am. Chem. Soc.* **1965**, *87* (9), 2045–2046. https://doi.org/10.1021/ja01087a033.

(97) Hirao, H. Correlation Diagram Approach as a Tool for Interpreting Chemistry: An Introductory Overview. *Wiley Interdisciplinary Reviews: Computational Molecular Science* **2011**, *1* (3), 337–349. https://doi.org/10.1002/wcms.20.

(98) Woodward, R. B.; Hoffmann, R. *The Conservation of Orbital Symmetry*; Elsevier, 1971. https://doi.org/10.1016/C2013-0-12537-8.

(99) Schmidt, W. Competition between Concerted and Non-Concerted Pathways in Symmetry-Forbidden Reactions. *Tetrahedron Letters* **1972**, *13* (7), 581–584. https://doi.org/10.1016/S0040-4039(01)84383-5.

(100) Saima, B.; Khan, A.; Nisa, R. U.; Mahmood, T.; Ayub, K. Theoretical Insights into Thermal Cyclophanediene to Dihydropyrene Electrocyclic Reactions; a Comparative Study of Woodward Hoffmann Allowed and Forbidden Reactions. *J Mol Model* **2016**, *22* (4), 1–9. https://doi.org/10.1007/s00894-016-2948-6.

(101) Bernardi, F.; Olivucci, M.; Robb, M. Modelling Photochemical Reactivity of Organic Systems — A New Challenge to Quantum Computational Chemistry. *Israel Journal of Chemistry* **1993**, *33* (3), 265–276. https://doi.org/10.1002/ijch.199300033.

(102) Celani, P.; Garavelli, M.; Ottani, S.; Bernardi, F.; Robb, M. A.; Olivucci, M. Molecular "Trigger" for the Radiationless Deactivation of Photoexcited Conjugated Hydrocarbons. *Journal of the American Chemical Society* **1995**, *117* (46), 11584–11585.

(103) Garavelli, M.; Smith, B. R.; Bearpark, M. J.; Bernardi, F.; Olivucci, M.; Robb, M. A. Relaxation Paths and Dynamics of Photoexcited Polyene Chains: Evidence for Creation and Annihilation of Neutral Soliton Pairs. *J. Am. Chem. Soc.* **2000**, *122* (23), 5568–5581. https://doi.org/10.1021/ja000385l.

(104) Boggio-Pasqua, M.; Ravaglia, M.; Bearpark, M. J.; Garavelli, M.; Robb, M. A. Can

Diarylethene Photochromism Be Explained by a Reaction Path Alone? A CASSCF Study with Model MMVB Dynamics. *J. Phys. Chem. A* **2003**, *107* (50), 11139–11152. https://doi.org/10.1021/jp036862e.

(105) Garavelli, M. Computational Organic Photochemistry: Strategy, Achievements and Perspectives. *Theoretical Chemistry Accounts* **2006**, *116* (1–3), 87–105. https://doi.org/10.1007/s00214-005-0030-z.

(106) Vanni, S.; Garavelli, M.; Robb, M. A. A New Formulation of the Phase Change Approach in the Theory of Conical Intersections. *Chemical Physics* **2008**, *347* (1–3), 46–56. https://doi.org/10.1016/j.chemphys.2007.09.055.

(107) Robb, M. A. In This Molecule There Must Be a Conical Intersection. In *Advances in Physical Organic Chemistry*; Elsevier, 2014; Vol. 48, pp 189–228. https://doi.org/10.1016/B978-0-12-800256-8.00003-5.

(108) Boggio-Pasqua, M. Computational Methods and Photochromism. In *Molecular Photoswitches*; John Wiley & Sons, Ltd, 2022; pp 19–37. https://doi.org/10.1002/9783527827626.ch2.

(109) Barbatti, M.; Paier, J.; Lischka, H. Photochemistry of Ethylene: A Multireference Configuration Interaction Investigation of the Excited-State Energy Surfaces. *The Journal of Chemical Physics* **2004**, *121* (23), 11614–11624. https://doi.org/10.1063/1.1807378.

(110) Gozem, S.; Huntress, M.; Schapiro, I.; Lindh, R.; Granovsky, A. A.; Angeli, C.; Olivucci, M. Dynamic Electron Correlation Effects on the Ground State Potential Energy Surface of a Retinal Chromophore Model. *J. Chem. Theory Comput.* **2012**, *8* (11), 4069–4080. https://doi.org/10.1021/ct3003139.

(111) Boggio-Pasqua, M.; Bearpark, M. J.; Klene, M.; Robb, M. A. A Computational Strategy for Geometry Optimization of Ionic and Covalent Excited States, Applied to Butadiene and Hexatriene. *J. Chem. Phys.* **2004**, *120* (17), 7849–7860. https://doi.org/10.1063/1.1690756.

(112) Santolini, V.; Malhado, J. P.; Robb, M. A.; Garavelli, M.; Bearpark, M. J. Photochemical Reaction Paths of Cis-Dienes Studied with RASSCF: The Changing Balance between Ionic and Covalent Excited States. *Molecular Physics* **2015**, *113* (13–14), 1978–1990. https://doi.org/10.1080/00268976.2015.1025880.

(113) Loos, P.-F.; Boggio-Pasqua, M.; Scemama, A.; Caffarel, M.; Jacquemin, D. Reference Energies for Double Excitations. *Journal of Chemical Theory and Computation* **2019**, *15* (3), 1939–1956. https://doi.org/10.1021/acs.jctc.8b01205.

(114) Lee, S.; Filatov, M.; Lee, S.; Choi, C. H. Eliminating Spin-Contamination of Spin-Flip Time Dependent Density Functional Theory within Linear Response Formalism by the Use of Zeroth-Order Mixed-Reference (MR) Reduced Density Matrix. *The Journal of Chemical Physics* **2018**, *149* (10), 104101. https://doi.org/10.1063/1.5044202.

(115) Becke, A. D. A New Mixing of Hartree–Fock and Local Density-functional Theories. *J. Chem. Phys.* **1993**, *98* (2), 1372–1377. https://doi.org/10.1063/1.464304.

(116) Rinkevicius, Z.; Vahtras, O.; Ågren, H. Spin-Flip Time Dependent Density Functional Theory Applied to Excited States with Single, Double, or Mixed Electron Excitation Character. *J. Chem. Phys.* **2010**, *133* (11), 114104. https://doi.org/10.1063/1.3479401.

(117) Krishnan, R.; Binkley, J. S.; Seeger, R.; Pople, J. A. Self-consistent Molecular Orbital Methods. XX. A Basis Set for Correlated Wave Functions. *J. Chem. Phys.* **1980**, *72* (1), 650–654. https://doi.org/10.1063/1.438955.

(118) Bakkar, A.; Lafolet, F.; Boggio-Pasqua, M.; Jouvenot, D.; Saint-Aman, E.; Cobo, S. Electrochemical Control of the Switching Process of Photochromic Dimethyldihydropyrene Derivatives. *Chemical Communications* **2017**, *53* (67), 9360–9363. https://doi.org/10.1039/C7CC05223E.

(119) Lognon, E.; Heitz, M.-C.; Bakkar, A.; Cobo, S.; Loiseau, F.; Saint-Aman, E.; Royal, G.; Boggio-Pasqua, M. Dependency of the Dimethyldihydropyrene Photochromic Properties on the Number of Pyridinium Electron-Withdrawing Groups. *ChemPhysChem* **2020**, *21* (14), 1571–1577. https://doi.org/10.1002/cphc.202000304.

(120) Krylov, A. I.; Gill, P. M. W. Q-Chem: An Engine for Innovation. *Wiley Interdisciplinary Reviews: Computational Molecular Science* **2013**, *3* (3), 317–326. https://doi.org/10.1002/wcms.1122.

(121) Schmidt, M. W.; Baldridge, K. K.; Boatz, J. A.; Elbert, S. T.; Gordon, M. S.; Jensen, J. H.; Koseki, S.; Matsunaga, N.; Nguyen, K. A.; Su, S.; Windus, T. L.; Dupuis, M.; Montgomery, J. A. General Atomic and Molecular Electronic Structure System. *Journal of Computational Chemistry* **1993**, *14* (11), 1347–1363. https://doi.org/10.1002/jcc.540141112.

(122) Becke, A. D. Density-functional Thermochemistry. III. The Role of Exact Exchange. *J. Chem. Phys.* **1993**, *98* (7), 5648–5652. https://doi.org/10.1063/1.464913.

(123) Werner, H.-J.; Knowles, P. J.; Knizia, G.; Manby, F. R.; Schütz, M. Molpro: A General-Purpose Quantum Chemistry Program Package. *Wiley Interdisciplinary Reviews: Computational Molecular Science* **2012**, *2* (2), 242–253. https://doi.org/10.1002/wcms.82.

(124) Zobel, J. P.; Nogueira, J. J.; González, L. The IPEA Dilemma in CASPT2. *Chem. Sci.* **2017**, *8* (2), 1482–1499. https://doi.org/10.1039/C6SC03759C.

(125) Sarkar, R.; Loos, P.-F.; Boggio-Pasqua, M.; Jacquemin, D. Assessing the Performances of CASPT2 and NEVPT2 for Vertical Excitation Energies. *J. Chem. Theory Comput.* **2022**, *18* (4), 2418–2436. https://doi.org/10.1021/acs.jctc.1c01197.

(126) Malmqvist, P. Å.; Pierloot, K.; Shahi, A. R. M.; Cramer, C. J.; Gagliardi, L. The Restricted Active Space Followed by Second-Order Perturbation Theory Method: Theory and Application to the Study of CuO_2 and Cu_2O_2 Systems. *J. Chem. Phys.* **2008**, *128* (20), 204109. https://doi.org/10.1063/1.2920188.

(127) Sauri, V.; Serrano-Andrés, L.; Shahi, A. R. M.; Gagliardi, L.; Vancoillie, S.; Pierloot, K. Multiconfigurational Second-Order Perturbation Theory Restricted Active Space (RASPT2) Method for Electronic Excited States: A Benchmark Study. *J. Chem. Theory Comput.* **2011**, *7* (1),

153–168. https://doi.org/10.1021/ct100478d.

(128) Dunning, T. H. Gaussian Basis Sets for Use in Correlated Molecular Calculations. I. The Atoms Boron through Neon and Hydrogen. *J. Chem. Phys.* **1989**, *90* (2), 1007–1023. https://doi.org/10.1063/1.456153.

(129) Koch, H.; Christiansen, O.; Jørgensen, P.; Sanchez de Merás, A. M.; Helgaker, T. The CC3 Model: An Iterative Coupled Cluster Approach Including Connected Triples. *The Journal of Chemical Physics* **1997**, *106* (5), 1808–1818. https://doi.org/10.1063/1.473322.

(130) Loos, P.-F.; Scemama, A.; Blondel, A.; Garniron, Y.; Caffarel, M.; Jacquemin, D. A Mountaineering Strategy to Excited States: Highly Accurate Reference Energies and Benchmarks. *Journal of Chemical Theory and Computation* **2018**, *14* (8), 4360–4379. https://doi.org/10.1021/acs.jctc.8b00406.

(131) Loos, P.-F.; Lipparini, F.; Boggio-Pasqua, M.; Scemama, A.; Jacquemin, D. A Mountaineering Strategy to Excited States: Highly Accurate Energies and Benchmarks for Medium Sized Molecules. *Journal of Chemical Theory and Computation* **2020**, *16* (3), 1711–1741. https://doi.org/10.1021/acs.jctc.9b01216.

(132) Loos, P.-F.; Scemama, A.; Boggio-Pasqua, M.; Jacquemin, D. Mountaineering Strategy to Excited States: Highly Accurate Energies and Benchmarks for Exotic Molecules and Radicals. *Journal of Chemical Theory and Computation* **2020**, *16* (6), 3720–3736. https://doi.org/10.1021/acs.jctc.0c00227.

(133) Loos, P.-F.; Jacquemin, D. A Mountaineering Strategy to Excited States: Highly Accurate Energies and Benchmarks for Bicyclic Systems. *J. Phys. Chem. A* **2021**, *125* (47), 10174–10188. https://doi.org/10.1021/acs.jpca.1c08524.

(134) Véril, M.; Scemama, A.; Caffarel, M.; Lipparini, F.; Boggio-Pasqua, M.; Jacquemin, D.; Loos, P.-F. QUESTDB: A Database of Highly Accurate Excitation Energies for the Electronic Structure Community. *WIREs Computational Molecular Science* **2021**, *11* (5), e1517. https://doi.org/10.1002/wcms.1517.

(135) Matthews, D. A.; Cheng, L.; Harding, M. E.; Lipparini, F.; Stopkowicz, S.; Jagau, T.-C.; Szalay, P. G.; Gauss, J.; Stanton, J. F. Coupled-Cluster Techniques for Computational Chemistry: The CFOUR Program Package. *J. Chem. Phys.* **2020**, *152* (21), 214108. https://doi.org/10.1063/5.0004837.

(136) Tomasello, G.; Garavelli, M.; Orlandi, G. Tracking the Stilbene Photoisomerization in the S_1 State Using RASSCF. *Physical Chemistry Chemical Physics* **2013**, *15* (45), 19763. https://doi.org/10.1039/c3cp52310a.

(137) Park, J. W.; Shiozaki, T. On the Accuracy of Retinal Protonated Schiff Base Models. *Molecular Physics* **2018**, *116* (19–20), 2583–2590. https://doi.org/10.1080/00268976.2018.1457807.

(138) Nikiforov, A.; Gamez, J. A.; Thiel, W.; Huix-Rotllant, M.; Filatov, M. Assessment of Approximate Computational Methods for Conical Intersections and Branching Plane Vectors

in Organic Molecules. *J. Chem. Phys.* **2014**, *141* (12), 124122. https://doi.org/10.1063/1.4896372.

(139) Lee, S.; Shostak, S.; Filatov, M.; Choi, C. H. Conical Intersections in Organic Molecules: Benchmarking Mixed-Reference Spin–Flip Time-Dependent DFT (MRSF-TD-DFT) vs Spin–Flip TD-DFT. *The Journal of Physical Chemistry A* **2019**, *123* (30), 6455–6462. https://doi.org/10.1021/acs.jpca.9b06142.

(140) Winslow, M.; Cross, W. B.; Robinson, D. Comparison of Spin-Flip TDDFT-Based Conical Intersection Approaches with XMS-CASPT2. *Journal of Chemical Theory and Computation* **2020**, *16* (5), 3253–3263. https://doi.org/10.1021/acs.jctc.9b00917.

(141) Sarkar, R.; Heitz, M.-C.; Boggio-Pasqua, M. Absorption Band Structure of the Photochromic Dimethyldihydropyrene/Metacyclophanediene Couple. Insight from Vibronic Coupling Theory. *J. Chem. Phys.* **2022**, *157* (22), 224303. https://doi.org/10.1063/5.0125114.

TOC graphics.